MiR-342 controls *Mycobacterium tuberculosis* susceptibility by modulating inflammation and cell death

Beibei Fu[1,†], Xiaoyuan Lin[1,†], Shun Tan[2,†], Rui Zhang[3,†], Weiwei Xue[4], Haiwei Zhang[5], Shanfu Zhang[1], Qingting Zhao[1], Yu Wang[6], Kelly Feldman[7], Lei Shi[1], Shaolin Zhang[4], Weiqi Nian[5], Krishna Chaitanya Pavani[8], Zhifeng Li[1,9,*] 🔵, Xingsheng Wang[10,**] 🔵 & Haibo Wu[1,***] 🔵

Abstract

Tuberculosis (TB) is an infectious disease caused by *Mycobacterium tuberculosis* (Mtb) that places a heavy strain on public health. Host susceptibility to Mtb is modulated by macrophages, which regulate the balance between cell apoptosis and necrosis. However, the role of molecular switches that modulate apoptosis and necrosis during Mtb infection remains unclear. Here, we show that Mtb-susceptible mice and TB patients have relatively low miR-342-3p expression, while mice with miR-342-3p overexpression are more resistant to Mtb. We demonstrate that the miR-342-3p/SOCS6 axis regulates anti-Mtb immunity by increasing the production of inflammatory cytokines and chemokines. Most importantly, the miR-342-3p/SOCS6 axis participates in the switching between Mtb-induced apoptosis and necrosis through A20-mediated K48-linked ubiquitination and RIPK3 degradation. Our findings reveal several strategies by which the host innate immune system controls intracellular Mtb growth via the miRNA-mRNA network and pave the way for host-directed therapies targeting these pathways.

Introduction

Tuberculosis (TB) is a globally distributed infectious disease caused by *Mycobacterium tuberculosis* (Mtb). According to recent studies, more than one-quarter of the global human population has been infected with Mtb (Chakaya *et al*, 2021). However, only about 10% of infected individuals develop active TB, indicating that innate immunity likely plays a critical role in limiting Mtb replication.

MicroRNAs (miRNAs) act by negatively regulating the expression of key genes (Bartel, 2018). Some evidence indicates that host miRNAs may impact the microbial life cycle and pathogenesis (Jopling *et al*, 2005; Huang *et al*, 2007; Liu *et al*, 2016). More commonly, bacteria can regulate the expression of host-specific miRNAs and weaken the host's immunity to promote survival and immune evasion (Kumar *et al*, 2015; Liu *et al*, 2018; Fu *et al*, 2020a). Recently, it has also been reported that microbe-derived miRNAs have a negative effect on host antimicrobial immunity (Sullivan *et al*, 2005; Choy *et al*, 2008). Thus, both bacterial and host miRNAs are likely to influence the relationship between hosts and pathogens. It has been shown that miR-342-3p is involved in the immune response in a variety of diseases. For example, overexpression of miR-342-3p can greatly suppress the inflammatory response and lipid uptake in THP-1 cells and can therefore regulate the development of atherosclerosis (Wang *et al*, 2019). In a recent study, miR-342-3p was shown to play an anti-inflammatory role in regulatory T cells and to contribute to glucocorticoid-mediated treatment of inflammation in murine autoimmune models (Kim *et al*,

1   School of Life Sciences, Chongqing University, Chongqing, China
2   Chongqing Public Health Medical Center, Chongqing, China
3   Department of Respiratory Medicine, First Affiliated Hospital of Chongqing Medical University, Chongqing, China
4   School of Pharmaceutical Sciences, Chongqing University, Chongqing, China
5   Chongqing Key Laboratory of Translational Research for Cancer Metastasis and Individualized Treatment, Chongqing University Cancer Hospital, Chongqing, China
6   Technical Center of Chongqing Customs, Chongqing, China
7   Department of Molecular and Cell Biology, University of California, Berkeley, CA, USA
8   Department of Nutrition, Genetics and Ethology, Ghent University, Merelbeke, Belgium
9   Chongqing Center for Disease Control and Prevention, Chongqing, China
10 Department of Respiratory Medicine, Chongqing Emergency Medical Center, Affiliated Central Hospital of Chongqing University, Chongqing, China
    *Corresponding author. Tel: +86 23 68812969; E-mail: qc_zhifengli@126.com
    **Corresponding author. Tel: +86 23 63692253; E-mail: xingswang@163.com
    ***Corresponding author. Tel: +86 23 65678491; E-mail: hbwu023@cqu.edu.cn
    †These authors contributed equally to this work.

2020). However, the role of miR-342-3p in anti-tuberculosis immunity has not yet been reported.

SOCS proteins are negative regulators of the JAK/STAT pathway (Alexander & Hilton, 2004), and accumulating evidence indicates that they are involved in the control of the cytokine networks responsible for adequate and efficient innate immune responses (Yoshimura *et al*, 2007). For example, SOCS1 expression is significantly increased in patients with tuberculosis, where SOCS1 transcript levels are correlated with disease severity (Masood *et al*, 2012; Masood *et al*, 2013; Masood *et al*, 2014). SOCS1, 4, and 5 are highly expressed in mice infected with hypervirulent Mtb (Manca *et al*, 2005). CISH, a founding member of the SOCS family, can mediate control of Mtb in mice shortly after infection (Carow *et al*, 2017). Meanwhile, SOCS6 expression is reportedly enhanced by exosomes from IL-1β-primed mesenchymal stem cells; this process is related to osteoarthritic signal regulation (Kim *et al*, 2021). In addition, the homologs of vertebrate SOCS6 in *Eriocheir sinensis* are critical to the immune response to bacterial and viral infection (Qu *et al*, 2018). These studies suggest that SOCS6 may also play a role in inflammation and infection. However, to our knowledge, there are no currently published studies on the role of SOCS6 in the pathogenesis of tuberculosis.

C3HeB/FeJ (C3H) and C57BL/6J (B6) inbred mice are often used as models in TB susceptibility studies. C3H mice are extremely susceptible to virulent Mtb, have marked lung pathology, and die soon after infection with Mtb. In contrast, B6 mice, a substrain derived from C57BL/6 mice, have been reported to be resistant to Mtb (Kramnik *et al*, 2000; Pan *et al*, 2005; Kramnik, 2008). More specifically, after Mtb stimulation, C3H mouse bone marrow-derived macrophages (BMDMs) showed characteristic necrosis, whereas B6 BMDMs mainly underwent apoptosis. Previous studies also showed that extreme susceptibility to Mtb was associated with necrosis of Mtb-susceptible macrophages (Kramnik *et al*, 2000; Pan *et al*, 2005; Wu *et al*, 2015; Leu *et al*, 2017). The precise mechanism for this phenomenon, however, is not well understood. In this study, we used C3H and B6 inbred mice to demonstrate that miR-342-3p targets and represses *Socs6*, a negative regulator of cytokine signaling. We showed that the miR-342-3p/SOCS6 axis modulates anti-Mtb immunity by inducing production of inflammatory cytokines (TNF-α, IL-1, IL-6, and CXCL15) and chemokines (CCL5, CXCL10, and ICAM1). Most importantly, the miR-342-3p/SOCS6 axis is involved in the switching between Mtb-induced apoptosis and necrosis. Collectively, we have demonstrated a new regulatory pathway involved in tissue necrosis during Mtb infection. These findings suggest that new host-based therapies targeting these pathways might help combat drug-susceptible and drug-resistant TB.

Results

MiR-342-3p is associated with TB susceptibility

Our group has previously reported that array-based miRNA profiling can help to shed light on the role of miRNAs in the switching between Mtb-induced apoptosis and necrosis (Wu *et al*, 2016). We noticed that in macrophages with an Mtb-resistant phenotype, two of the five highly expressed miRNAs, miR-342-5p, and miR-342-3p, were spliced from the same precursor (NCBI Accession No.

PRJNA279232). Using C3H and B6 BMDMs, we first investigated whether miR-342 expression was correlated with Mtb infection in mouse macrophages. Semiquantitative RT–PCR analysis showed that the expression levels of primary (pri-), precursor (pre-), and mature miR-342 transcripts were upregulated in Mtb-stimulated B6 BMDMs but were not found in C3H BMDMs (Fig 1A). The relative levels of mature miR-342-5p and miR-342-3p in B6 and C3H BMDMs were then examined through northern blotting and quantitative RT–PCR (qRT–PCR). The results showed that miR-342-5p and miR-342-3p expression was much higher in B6 BMDMs than in C3H BMDMs (Fig 1B and C).

Next, a microRNA mimic and inhibitor were used to investigate whether miR-342 was related to the Mtb-resistant phenotype. The mechanism of cell death in Mtb-infected wild-type C3H and B6 BMDMs is verified in Fig EV1A, and the effectiveness of the miR-342-3p mimic and inhibitor is verified in Fig EV1B. Transfection of C3H BMDMs with the miR-342-3p mimic switched Mtb-induced necrosis to caspase-dependent cell apoptosis; this switching was inhibited by benzyloxycarbonyl-Val-Ala-Asp-fluoromethylketone (zVAD, a pan-caspase inhibitor (Zhang *et al*, 2009)) (Figs 1D and E, and EV1C). On the other hand, inhibition of miR-342-3p in B6 BMDMs turned Mtb-induced apoptosis into caspase-independent necrosis (Figs 1F and EV1D), and cells treated with both Mtb and zVAD showed decreased cell viability (Fig 1G). Furthermore, transfection of C3H BMDMs with the miR-342-3p mimic significantly hindered Mtb growth (Fig 1H), while inhibition of miR-342-3p in B6 BMDMs increased Mtb survival and replication (Fig 1I). In addition, treatment of C3H BMDMs with the miR-342-3p inhibitor resulted in more severe necrosis, while treatment of B6 BMDMs with the miR-342-3p mimic resulted in a greater degree of apoptosis (Fig EV1E–H). Since the other splicing product, miR-342-5p, showed no significant effect on the mechanisms of cell death (Fig EV1I and J), we chose to further investigate miR-342-3p. As miR-342-3p is conserved between mice and humans, we analyzed the production of miR-342-3p in peripheral blood mononuclear cells (PBMCs) from 34 TB patients. We observed that TB patients expressed relatively low levels of miR-342-3p (Fig 1J). These results suggest that miR-342-3p may act as a positive regulator of the immune response to Mtb infection.

MiR-342-3p enhances the production of inflammatory cytokines

We generated a *Mir342*^+/+^ C3H mouse strain carrying the pBROAD3-miR-342 sequence and a *Mir342*^−/−^ B6 mouse strain with knockout of the pre-miR-342 sequence (Appendix Fig S1A and B). Compared to the control group, the survival time of *Mir342*^+/+^ C3H mice infected with 400 CFU Mtb was significantly lengthened (Fig 2A), while the survival time of Mtb-infected *Mir342*^−/−^ B6 mice was remarkably shortened (Fig 2B). We also observed a statistically significant difference in bacterial loads in the lungs, spleens, and livers of *Mir342*^+/+^ C3H mice and their wild-type littermates (C3H) (Fig 2C) as well as *Mir342*^−/−^ B6 mice and their wild-type littermates (B6) (Fig 2D). *Mir342*^−/−^ B6 mice developed massive necrotic lung lesions after intravenous infection (Fig 2E, Appendix Table S1). In contrast, Mtb-infected *Mir342*^+/+^ C3H mice did not develop any lung lesions and only displayed trace levels of inflammation (Fig 2F, Appendix Table S1). Next, we detected the expression of inflammatory cytokines secreted by
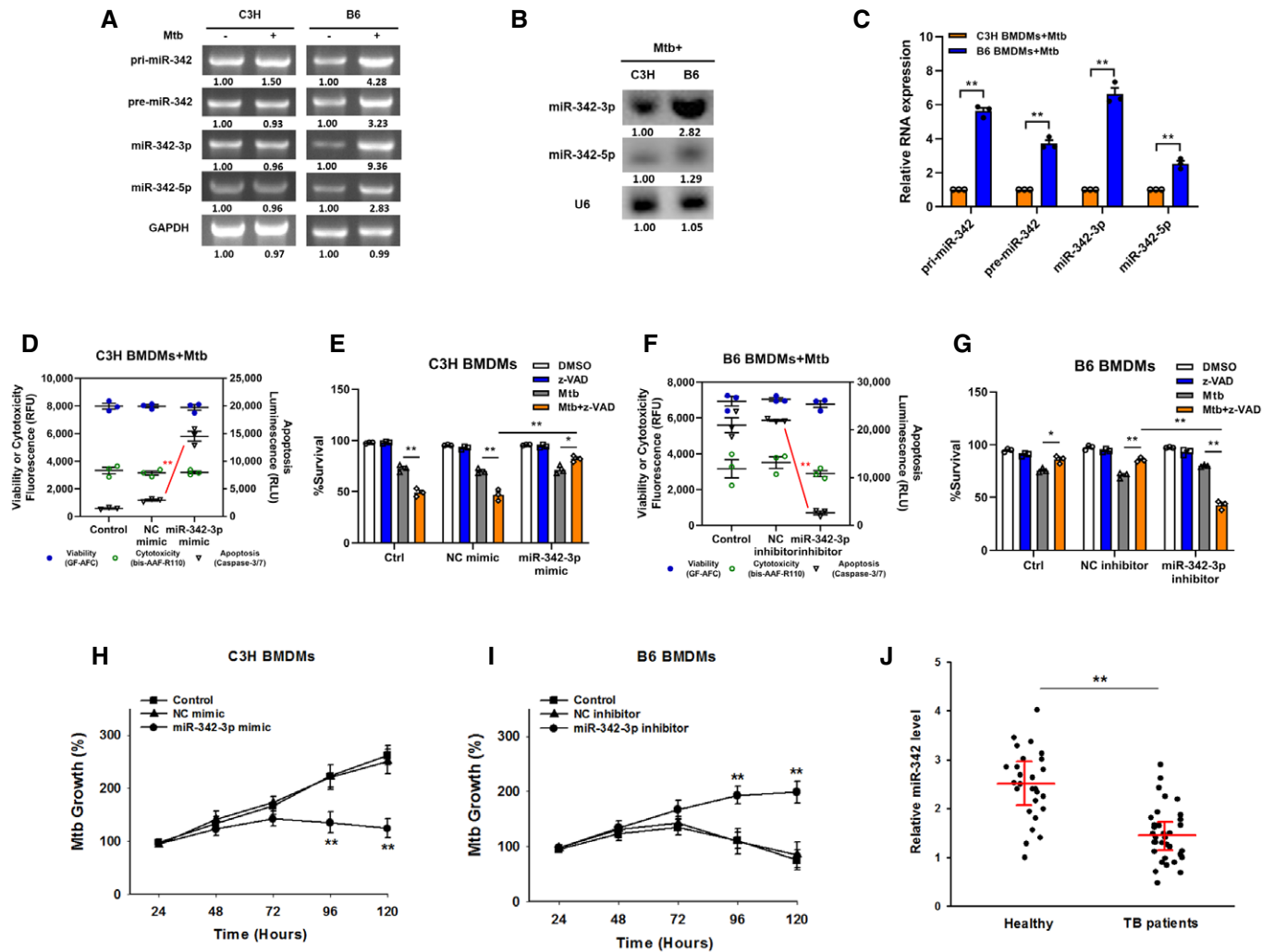
Figure 1. MiR-342-3p associates with TB susceptibility.

A   Expression changes of pri-, pre-, and mature miR-342 transcripts were analyzed by semiquantitative PCR in C3H or B6 BMDMs after Mtb infection. Representative blots from $n = 3$ biological replicates are shown.

B, C   The relative expressions of miR-342-3p and miR-342-5p were analyzed by northern blotting (B, representative blots from $n = 3$ biological replicates are shown) or quantitative real-time PCR (C, data are shown as the mean $\pm$ SEM of $n = 3$ biological replicates) in Mtb-stimulated C3H and B6 BMDMs.

D–G   Cell death mechanisms of C3H BMDMs transfected with miR-342-3p mimic (D), or B6 BMDMs transfected with miR-342-3p inhibitor (F), followed by Mtb infection for 36 h. Cell viabilities of C3H BMDMs transfected with miR-342-3p mimic (E), or B6 BMDMs transfected with miR-342-3p inhibitor (G), followed by stimulation with Mtb or z-VAD (20 µM) for 24 h. Data are shown as the mean $\pm$ SEM of $n = 3$ biological replicates.

H, I   Mtb growth rates of C3H BMDMs transfected with miR-342-3p mimic (H), or B6 BMDMs transfected with miR-342-3p inhibitor (I) after Mtb infection. Data are shown as the mean $\pm$ SEM of $n = 3$ biological replicates.

J   Expression levels of miR-342-3p in PBMCs from healthy controls ($n = 27$) or TB patients ($n = 34$) were detected by qRT–PCR. Data are shown as the medians $\pm$ interquartile ranges.

Data information: ANOVA followed by Bonferroni post *hoc* test (C-I) and Mann–Whitney *U* test (J) were used for data analysis. *$P < 0.05$, **$P < 0.01$. Abbreviation: NC, negative control.

Source data are available online for this figure.

BMDMs during Mtb infection. Compared with littermate controls, $Mir342^{+/+}$ C3H mice secreted increased levels of TNF-α, IL-1, IL-6, and CXCL15 (also known as IL-8) (Fig 2G). Deletion of miR-342 in B6 mice resulted in disordered cytokine secretion (Fig 2H). Taken together, these data indicate that miR-342-3p plays an important role in the switch between necrosis and apoptosis in Mtb-infected BMDMs and has a profound effect on anti-tuberculosis immunity.

MiR-342-3p directly targets SOCS6 to regulate anti-Mtb immunity

The targets of miR-342-3p were predicted using the PicTar, miRanda, and TargetScan databases. We narrowed the candidate targets to dozens of molecules that may regulate the innate immune response (Fig EV2A). Using an siRNA screening strategy, we chose *Socs6* for further investigation based on its effect on the
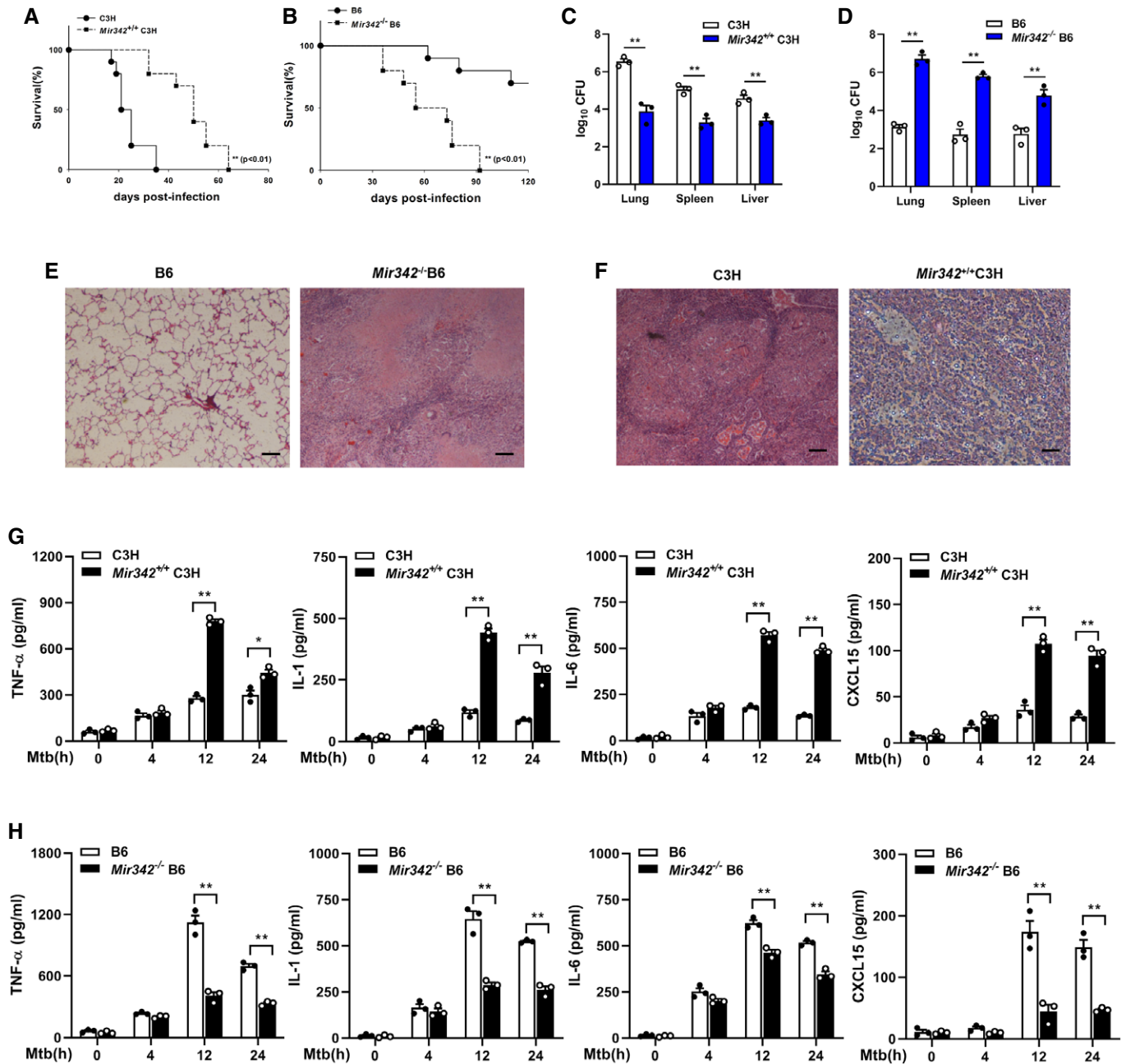
Figure 2. MiR-342-3p enhances the production of inflammatory cytokines.

A, B Survival of *Mir342*$^{+/+}$ C3H mice and their wild-type littermate controls (C3H) (n = 10) (A), or *Mir342*$^{-/-}$ B6 mice and their wild-type littermate controls (B6) (n = 10) (B) after aerosol infection with around 400 CFU Mtb. Data are shown as the Kaplan–Meier curves.

C, D Mtb bacterial loads in lungs, spleens, and livers of *Mir342*$^{+/+}$ C3H mice and their littermates (C3H) (C), or *Mir342*$^{-/-}$ B6 mice and their littermates (B6) at 21 days post-infection (dpi). Data are shown as the medians ± interquartile ranges of n = 3 biological replicates.

E, F Tuberculosis lung lesions of *Mir342*$^{-/-}$ B6 mice and their littermates (B6) (E), or *Mir342*$^{+/+}$ C3H mice and their littermates (C3H) (F) were detected by hematoxylin/eosin staining at 21 dpi. Representative images from n = 3 biological replicates are shown. Scale bar = 100 μm.

G, H Secretion of cytokines TNF-α, IL-1, IL-6, and CXCL15 in BMDMs obtained from *Mir342*$^{+/+}$ C3H and their littermates (C3H) (G), or from *Mir342*$^{-/-}$ B6 and their littermates (B6) (H) after Mtb stimulation, was detected by ELISA. Data are shown as the mean ± SEM of n = 3 biological replicates.

Data information: Log-rank (Mantel–Cox) test (A, B), Mann–Whitney U test (C, D), and ANOVA followed by Bonferroni post *hoc* test (G, H) were used for data analysis. *P < 0.05, **P < 0.01.

switching between Mtb-induced apoptosis and necrosis (Fig EV2B). The 3′-UTR of murine *Socs6* contains putative regions that match the miR-342-3p seed sequence (Fig 3A). To confirm the predicted regions, these putative matching sequences were amplified and inserted into a psicheck-2 vector. The vectors were then transfected into HEK-293T cells for dual-luciferase reporter (DLR) analysis. Our results showed that the miR-342-3p mimic dramatically suppressed the activity of the wild-type *Socs6* 3′-UTR but

not that of the double-mutation type (MUT) group (site 1 + 2 mut) (Fig 3B). qRT–PCR and Western blotting results showed that the miR-342-3p mimic considerably decreased SOCS6 mRNA and protein levels (Figs 3C and D, and EV2C and D), indicating that silencing was achieved through a combination of translation repression and mRNA destabilization (Jonas & Izaurralde, 2015). The RNA-induced silencing complex (RISC) has been reported to mediate the binding of miRNAs and mRNAs and activate Ago
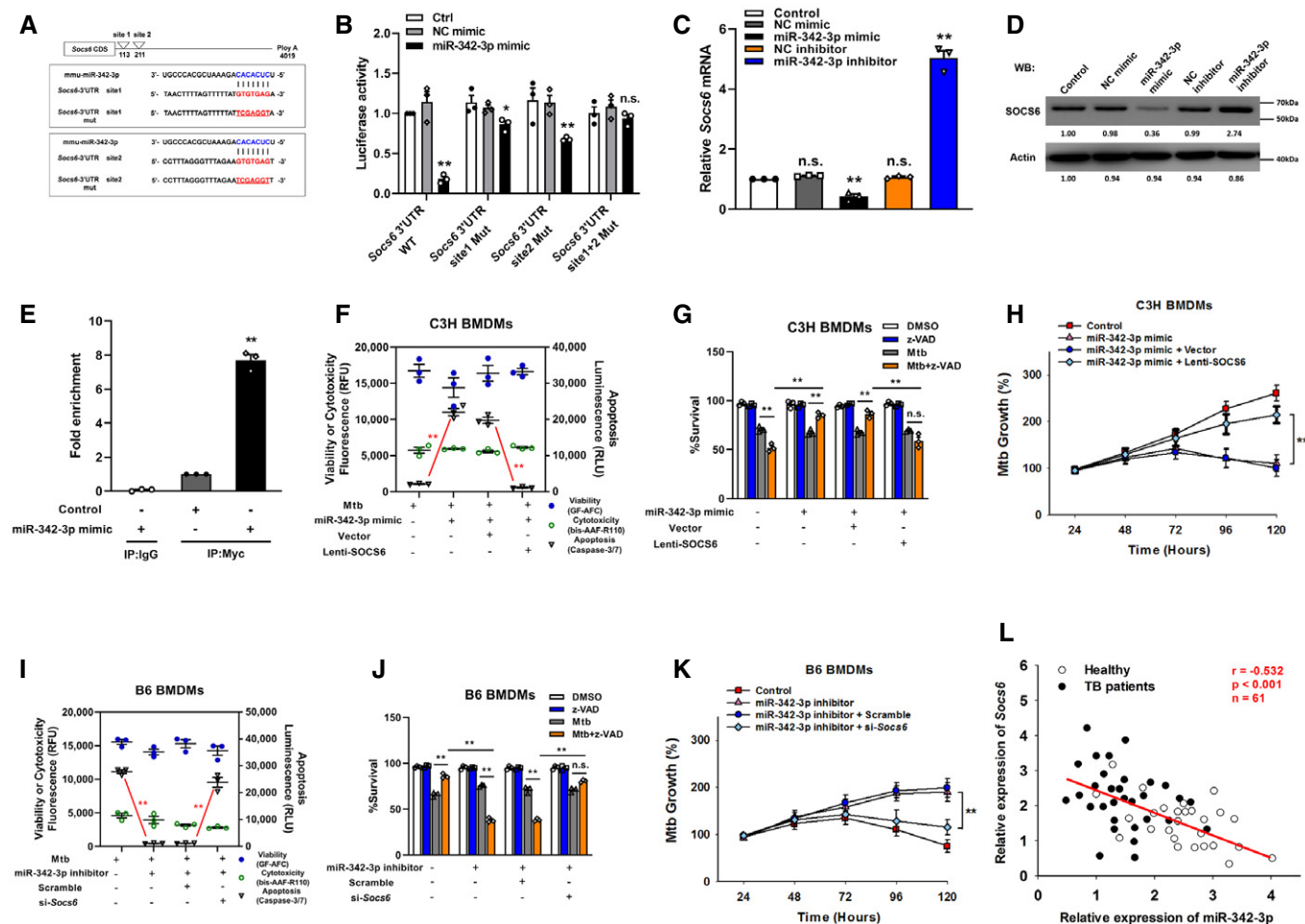
Figure 3. MicroRNA-342-3p directly targets SOCS6.

A Predicted binding sites of miR-342-3p and *Socs6* 3′-UTR.

B HEK-293T fibroblasts were cotransfected with miR-342-3p mimic and luciferase reporter construct containing wild-type or mutated UTR. After 24 h, cells were collected for luciferase assays. The Y-axis showed relative luciferase activity. Data are shown as the mean ± SEM of *n* = 3 biological replicates.

C, D MiR-342-3p mimic or inhibitor was transfected to NIH-3T3 fibroblasts. After 48 h, cells were collected for qRT–PCR (C, data are shown as the mean ± SEM of *n* = 3 biological replicates) and Western blotting (D, representative blots from *n* = 3 biological replicates are shown) to detect SOCS6 expression.

E € RAW264.7 cells were transfected with Myc-tagged Ago2 in the presence of miR-342-3p mimic or scramble for 24 h. Immunoprecipitation was performed with Myc antibody or IgG, and *Socs6* mRNA was detected by qRT–PCR. Data are shown as the mean ± SEM of *n* = 3 biological replicates.

F–H C3H BMDMs were transfected with miR-342-3p mimic or SOCS6-overexpressing lentivirus, followed by stimulation with Mtb or z-VAD (20 μM) for 24 h. Cell death mechanisms (F), cell viabilities (G), and Mtb growth rates (H) were analyzed, respectively. Data are shown as the mean ± SEM of *n* = 3 biological replicates.

I–K B6 BMDMs were transfected with miR-342-3p inhibitor or *Socs6* siRNA, followed by stimulation with Mtb or z-VAD (20 μM) for 24 h. Cell death mechanisms (I), cell viabilities (J), and Mtb growth rates (K) were analyzed, respectively. Data are shown as the mean ± SEM of *n* = 3 biological replicates.

L Relative expressions of miR-342-3p and *Socs6* in PBMCs from healthy individuals (*n* = 27) and TB patients (*n* = 34) were detected by qRT–PCR. The correlation between miR-342-3p and *Socs6* was analyzed by Spearman test. Spearman rank correlation: $r = -0.532$, $P < 0.001$, $n = 61$.

Data information: ANOVA followed by Bonferroni post *hoc* test (B, C, E-K) was used for data analysis. *$P < 0.05$, **$P < 0.01$. Abbreviations: *n.s.*, not significant. NC, negative control.

Source data are available online for this figure.
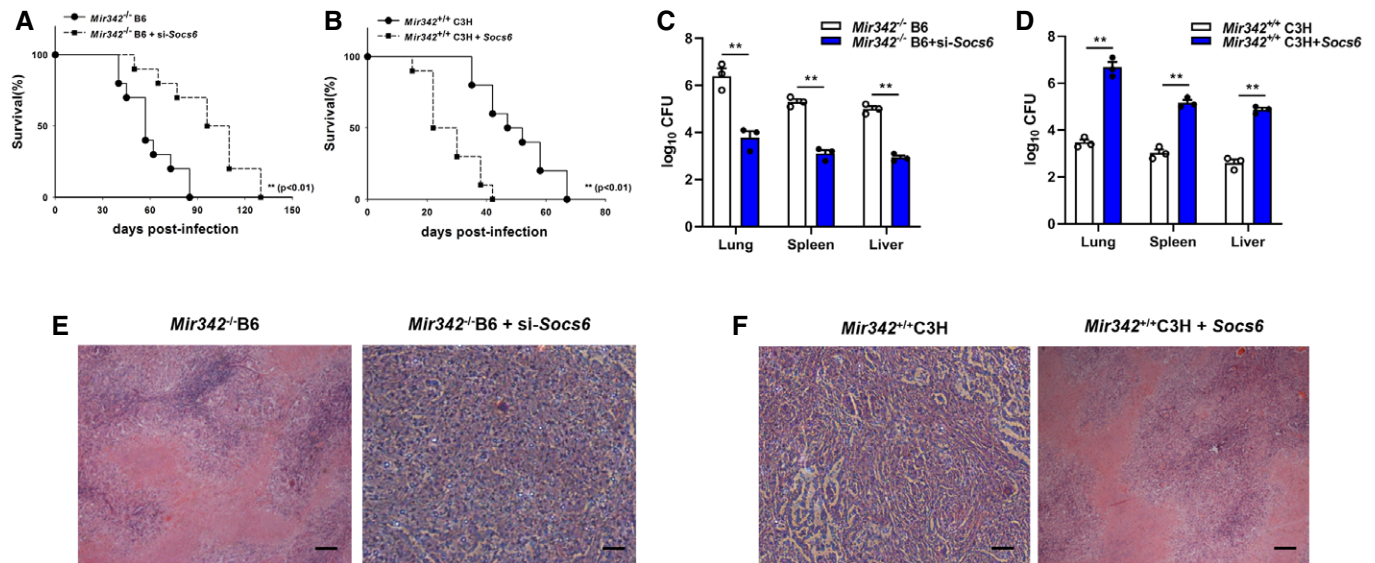
Figure 4. SOCS6 participates in anti-Mtb immunity.

A, B   Survival of $Mir342^{-/-}$ B6 and $Mir342^{-/-}$ B6 mice supplemented with $Socs6$ siRNA ($n = 10$) (A), or $Mir342^{+/+}$ C3H and $Mir342^{+/+}$ C3H mice supplemented with SOCS6-overexpressing vector ($n = 10$) (B), after aerosol infection with around 400 CFU Mtb. Data are shown as the Kaplan–Meier curves.

C, D   Mtb bacterial loads in lungs, spleens, and livers of $Mir342^{-/-}$ B6 and $Mir342^{-/-}$ B6 mice supplemented with $Socs6$ siRNA (C), or $Mir342^{+/+}$ C3H and $Mir342^{+/+}$ C3H mice supplemented with SOCS6-overexpressing vector (D) at 21 dpi. Data are shown as the medians $\pm$ interquartile ranges of $n = 3$ biological replicates.

E, F   Tuberculosis lung lesions of $Mir342^{-/-}$ B6 and $Mir342^{-/-}$ B6 mice supplemented with $Socs6$ siRNA (E), or $Mir342^{+/+}$ C3H and $Mir342^{+/+}$ C3H mice supplemented with SOCS6-overexpressing vector (F) at 21 dpi were detected by hematoxylin/eosin staining. Representative images from $n = 3$ biological replicates are shown. Scale bar = 100 μm.

Data information: Log-rank (Mantel–Cox) test (A, B) and Mann–Whitney U test (C, D) were used for data analysis. **$P < 0.01$.

(Iwakawa & Tomari, 2015). Therefore, RAW264.7 cells were transfected with a Myc-tagged Ago2 construct and a miR-342-3p mimic. Immunoprecipitation was performed using a Myc antibody, and $Socs6$ enrichment was determined by qRT–PCR. Cells transfected with the miR-342-3p mimic showed significant $Socs6$ mRNA enrichment compared with cells transfected with the scramble mimic (Fig 3E). These data indicated that $Socs6$ is a specific degradation target of miR-342-3p. Additionally, we discovered that restoration of SOCS6 expression abrogated the effects of miR-342-3p on cell death (Figs 3F and EV2E), cell survival (Fig 3G) and Mtb growth (Fig 3H) in C3H BMDMs. Moreover, the anti-tuberculosis effects of B6 BMDMs, which could be suppressed using the miR-342-3p inhibitor, were recovered upon siRNA-mediated SOCS6 knockdown (Figs 3I–K and EV2F). Meanwhile, we analyzed the relative expression of miR-342-3p and $Socs6$ in 27 healthy individuals and 34 TB patients and found an inverse correlation between miR-342-3p and

$Socs6$ (Spearman rank correlation: $r = -0.532$, $P < 0.001$, $n = 61$) (Fig 3L).

To confirm our findings, mice were intravenously infected with plasmids encoding SOCS6 or $Socs6$ siRNA (Fig EV2G and H). Survival time was lengthened in $Mir342^{-/-}$ B6 mice transfected with $Socs6$ siRNA, with lower bacterial loads in the indicated organs (Fig 4A and C). We also observed that survival time was shortened in $Mir342^{+/+}$ C3H mice transfected with the SOCS6-overexpressing vector, with significantly higher bacterial loads in the indicated organs (Fig 4B and D). Additionally, $Mir342^{-/-}$ B6 mice with $Socs6$ knockdown showed pulmonary inflammation rather than extensive TB nodules (Fig 4E, Appendix Table S1), while the lungs of $Mir342^{+/+}$ C3H mice transfected with SOCS6-overexpressing vector developed severe necrotic lesions (Fig 4F, Appendix Table S1). Furthermore, the alveolar macrophages from $Mir342^{-/-}$ B6 mice with $Socs6$ knockdown showed characteristic apoptosis, whereas

Figure 5. SOCS6 regulates the expression of chemokines via modulating JAK/STAT signaling.

A   ELISA was performed to detect the secretion of cytokines TNF-α, IL-1, IL-6, and CXCL15 in $Socs6^{+/+}$ and $Socs6^{-/-}$ BMDMs during Mtb stimulation. Data are shown as the mean $\pm$ SEM of $n = 3$ biological replicates.

B   Phosphorylation states of STAT1 in response to Mtb stimulation in $Socs6^{-/-}$ BMDMs were examined by Western blotting. Fludarabine treatment concentration was 10 μM, and the treatment time was 24 h. Representative blots from $n = 3$ biological replicates are shown.

C–F   Relative expressions of chemokines CCL5, CXCL10, ICAM1 (C), and caspase 3, caspase 7, caspase 8 (F) in Mtb-stimulated $Socs6^{+/+}$ or $Socs6^{-/-}$ BMDMs were detected by qRT–PCR. Data are shown as the mean $\pm$ SEM of $n = 3$ biological replicates. Cluster analysis of clinical samples. Heat maps showed relatively high (red) or low (green) expression levels of $Socs6$ and inflammatory factors in PBMCs from healthy individuals ($n = 27$) (D) and TB patients ($n = 34$) (E).

Data information: ANOVA followed by Bonferroni post hoc test (A, C, F) was used for data analysis. **$P < 0.01$. Abbreviation: $n.s.$, not significant.
Source data are available online for this figure.

▶
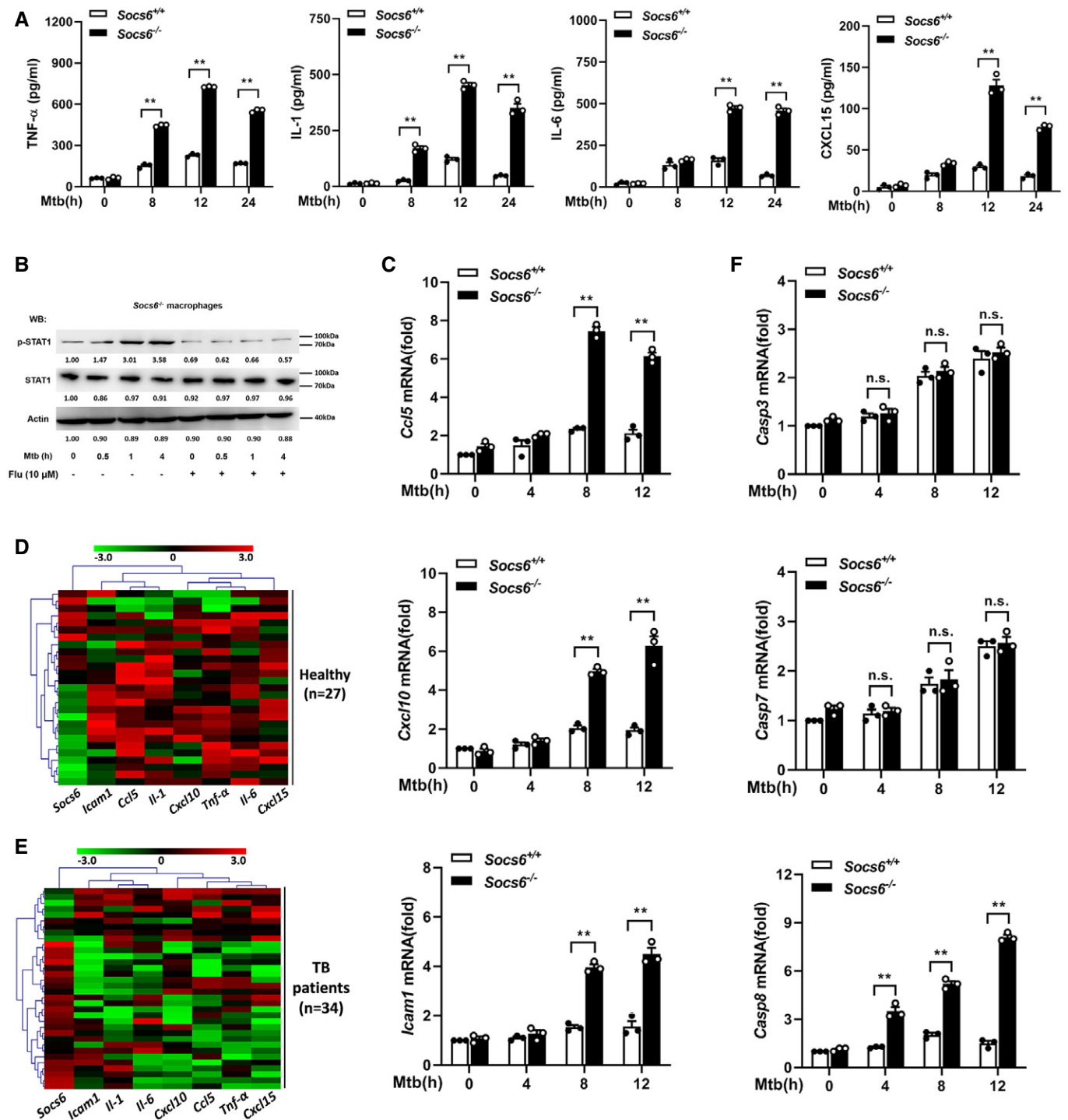
Figure 5.

those from $Mir342^{+/+}$ C3H mice with SOCS6 overexpression mainly underwent necrosis (Fig EV2I). We also detected the expression of inflammatory cytokines. As expected, TNF-α, IL-1, IL-6, and CXCL15 secretion was enhanced by SOCS6 knockdown in $Mir342^{-/-}$ B6 mice and hampered by SOCS6 overexpression in $Mir342^{+/+}$ C3H mice (Fig EV2J and K). Taken together, these data suggest that *Socs6* is a direct target of miR-342-3p and is responsible for anti-tuberculosis immunity in macrophages.

SOCS6 regulates the expression of chemokines by modulating JAK/STAT signaling

As a suppressor of cytokine signaling, SOCS6 can directly suppress the production of cytokines (Yoshimura *et al*, 2007). To gain insight into the role of *Socs6* in the innate immune response, we measured the release of cytokines in BMDMs obtained from Mtb-infected $Socs6^{+/+}$ and $Socs6^{-/-}$ mice. The release of TNF-α, IL-1, IL-6, and
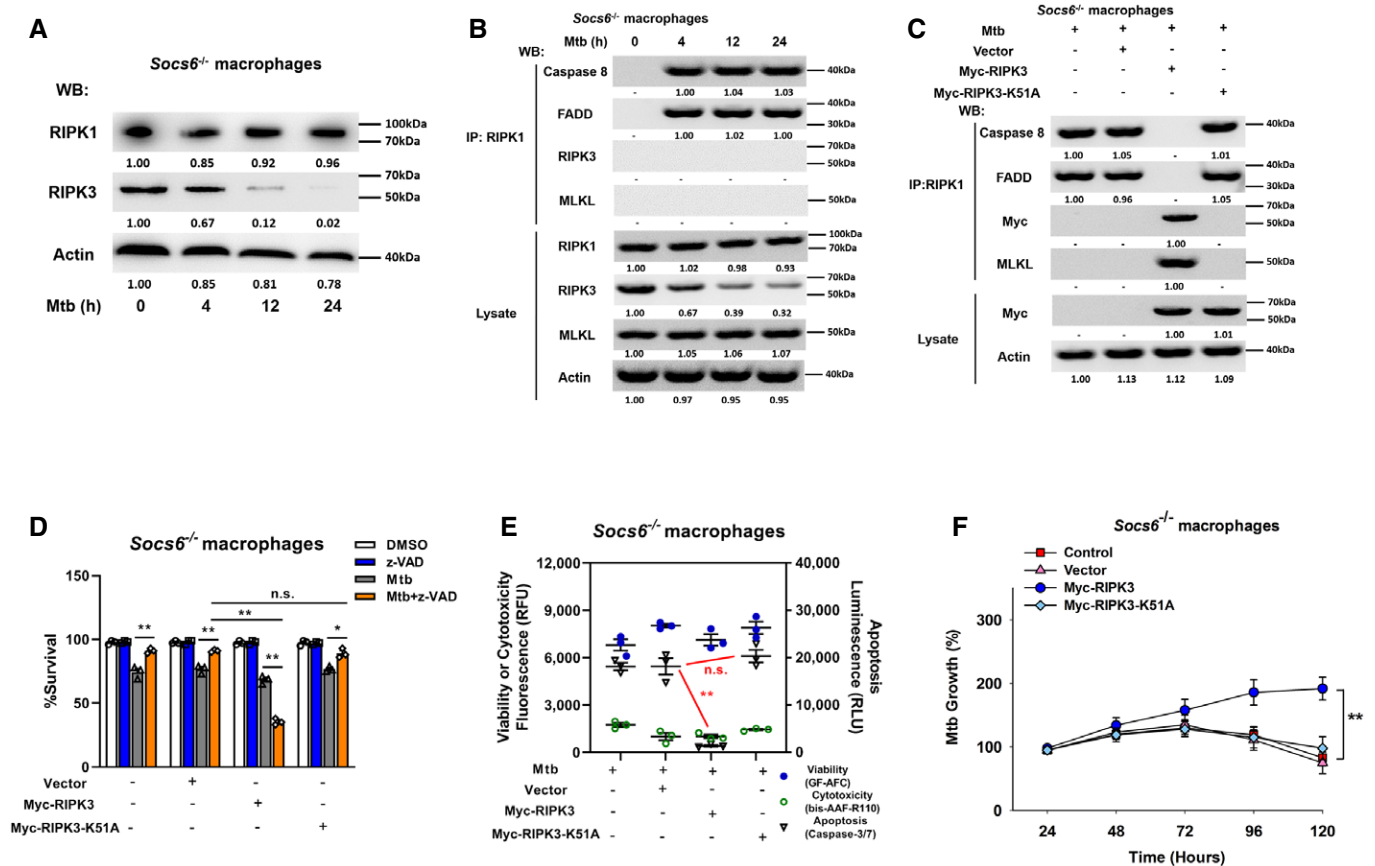
Figure 6. SOCS6 determines cell death mechanisms via modulating recruitment of RIPK3.

A Relative expressions of RIPK1 and RIPK3 were analyzed by Western blotting in $Socs6^{-/-}$ BMDMs stimulated with Mtb for 0–24 h. Representative blots from $n = 3$ biological replicates are shown.

B $Socs6^{-/-}$ BMDMs were stimulated with Mtb for 0–24 h, cell lysates were collected and immunoprecipitated using an anti-RIPK1 antibody. The recruitment of caspase 8, RIPK3, FADD, and MLKL was analyzed by immunoblots. The lower panel represents the immunoblot analysis of whole cell lysates. Representative blots from $n = 3$ biological replicates are shown.

C $Socs6^{-/-}$ BMDMs were transfected with plasmids expressing Myc-RIPK3 or Myc-RIPK3 K51A mutant for 24 h. Afterward, transfected cells were stimulated with Mtb for 12 h, and cell lysates were collected and immunoprecipitated using an anti-RIPK1 antibody. The recruitment of caspase 8, RIPK3, FADD, and MLKL was analyzed by immunoblot. The lower panel represents the immunoblot analysis of whole cell lysates. Representative blots from $n = 3$ biological replicates are shown.

D–F Cell viabilities (D), cell death mechanisms (E), or Mtb growth rates (F) of Mtb-infected $Socs6^{-/-}$ BMDMs that were transfected with plasmids expressing Myc-RIPK3 or Myc-RIPK3 K51A mutant as indicated. Z-VAD treatment concentration was 20 μM and the treatment time was 24 h. Data are shown as the mean ± SEM of $n = 3$ biological replicates.

Data information: ANOVA followed by Bonferroni post *hoc* test (D-F) was used for data analysis. *$P < 0.05$, **$P < 0.01$. Abbreviation: *n.*s., not significant.
Source data are available online for this figure.

CXCL15 from Mtb-infected macrophages was enhanced in the absence of SOCS6 (Fig 5A). Since SOCS proteins are known to negatively regulate the JAK/STAT signaling pathway (Alexander & Hilton, 2004), we examined the phosphorylation levels of the STAT family in Mtb-infected $Socs6^{+/+}$ and $Socs6^{-/-}$ BMDMs. The results suggested that STAT1 might be negatively regulated by SOCS6 signaling (Fig EV3A). Furthermore, we discovered that STAT1 phosphorylation was dramatically upregulated in Mtb-infected $Socs6^{-/-}$ BMDMs and could be blocked by a specific STAT1 inhibitor called fludarabine (Figs 5B and EV3B). In contrast, there was no significant fluctuation in STAT1 phosphorylation in $Socs6^{+/+}$ BMDMs post-Mtb infection (Fig EV3C). STAT phosphorylation and nuclear translocation are key steps in the activation of the JAK/STAT signaling pathway. Therefore, we next detected the intracellular

localization of STAT1 by immunofluorescence. In Mtb-infected $Socs6^{+/+}$ BMDMs, fluorescence was mainly distributed in the cytoplasm (Fig EV3D). However, in infected $Socs6^{-/-}$ BMDMs, most of the fluorescence was nuclear (Fig EV3D). These results suggested that SOCS6 might prevent inflammation and promote bacterial growth by repressing STAT1. This was further confirmed by testing the expression of several interferon-stimulated genes that can be directly regulated by STAT1. Knocking out $Socs6$ augmented CCL5, CXCL10, and ICAM1 expression in Mtb-infected cells (Figs 5C and EV3E and F). We also evaluated the expression of $Socs6$ and inflammatory factors in clinical samples. Cluster analysis showed that, in both healthy and diseased patients, expression levels of $Socs6$ and inflammatory factors were inversely correlated. Specifically, compared to healthy individuals, most TB patients displayed
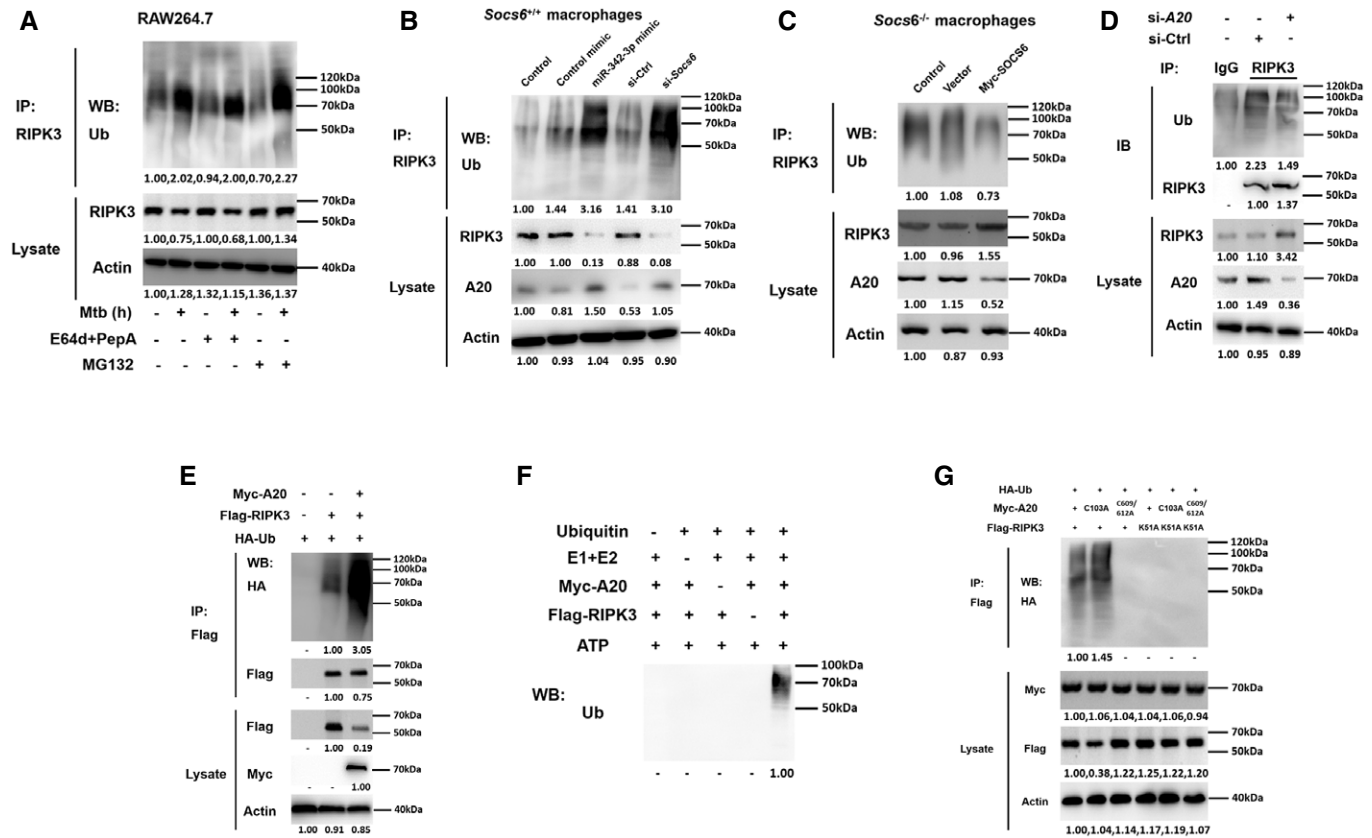
Figure 7. A20 controls degradation of RIPK3 through ubiquitin chains.

A   RAW264.7 cells were pretreated with or without E64d/PepA or MG132 for 4 h and then stimulated with or without Mtb for 12 h as indicated. Cell lysates were collected and immunoprecipitated using an anti-RIPK3 antibody, and the ubiquitination of endogenous RIPK3 was detected using an anti-Ub antibody. Representative blots from $n = 3$ biological replicates are shown.

B, C $Socs6^{+/+}$ BMDMs were transfected with miR-342-3p mimic or $Socs6$ siRNA (B), and $Socs6^{-/-}$ BMDMs were transfected with plasmid expressing Myc-SOCS6 (C) for 24 h as indicated. Transfected cells were then stimulated with Mtb for another 12 h, cell lysates were collected for immunoprecipitation, and ubiquitination of endogenous RIPK3 was detected by immunoblot. Representative blots from $n = 3$ biological replicates are shown.

D   RAW264.7 cells were transfected with $A20$ siRNA, and cell lysates were collected for immunoprecipitation and immunoblot. Representative blots from $n = 3$ biological replicates are shown.

E–G   RAW264.7 cells were transfected with plasmids expressing A20 and RIPK3 (E), or A20 and RIPK3 mutants (G) as indicated, cell lysates were collected for immunoprecipitation and immunoblot. Myc-A20 or Flag-RIPK3 purified from transfected HEK-293T cells was incubated with ATP, E1, E2, and ubiquitin as indicated. The $in\ vitro$ ubiquitination of RIPK3 was analyzed by immunoblot using an anti-Ub antibody (F). Representative blots from $n = 3$ biological replicates are shown.

Source data are available online for this figure.

relatively higher expression of $Socs6$ and lower expression of inflammatory factors (Fig 5D and E). Since the release of IFN-γ is closely related to Mtb infection, we tested whether SOCS6 regulated IFN-γ expression. The results showed that IFNγ expression was increased in both $Socs6^{+/+}$ and $Socs6^{-/-}$ cells following Mtb infection (Fig EV3G). Therefore, we hypothesize that SOCS6 does not play a role in the expression of IFN-γ. Additionally, since STAT1-mediated cell death is essential for host immunity against pathogens (O'Shea $et\ al$, 2015), we tested the expression of apoptosis-associated caspases, such as caspases 2, 3, 7, 8, and 9 (Fulda & Debatin, 2002; Sironi & Ouchi, 2004; Hong $et\ al$, 2019; Song $et\ al$, 2019). The results showed that Mtb-infected $Socs6^{+/+}$ and $Socs6^{-/-}$ BMDMs expressed significantly different levels of caspase 8 (Figs 5F and EV3E, F, H and I) and that these levels were specifically regulated by STAT1 (Fig EV3J and K). Collectively, these results indicate that the production of STAT1-mediated inflammatory factors plays

an important role in the SOCS6 regulatory network, which controls the immune response to Mtb infection.

SOCS6 regulates cell death mechanisms by modulating the recruitment of RIPK3

To understand the role of the cell death complex in the SOCS6 regulatory network, we analyzed the expression levels of RIPK1 and RIPK3 in Mtb-infected $Socs6^{+/+}$ and $Socs6^{-/-}$ BMDMs. Interestingly, RIPK3 was decreased in Mtb-infected $Socs6^{-/-}$ BMDMs, while RIPK1 was not affected by SOCS6 expression (Figs 6A and EV4A). To investigate the composition of the cell death complex during Mtb infection, we first infected $Socs6^{+/+}$ and $Socs6^{-/-}$ BMDMs with Mtb for 4–24 h and then performed immunoprecipitation for RIPK1 followed by immunoblotting for caspase 8, RIPK3, FADD, and MLKL. In $Socs6^{+/+}$ BMDMs, we detected formation of a

necrosis-related complex, whereas in $Socs6^{-/-}$ BMDMs, we observed assembly of the RIPK1-FADD-Caspase 8 complex, which can induce apoptosis (Figs 6B and EV4B). We then overexpressed either an empty vector or Myc-tagged RIPK3 in $Socs6^{-/-}$ BMDMs. Compared with the empty vector control, transfection of RIPK3 led to substantial recruitment of MLKL (Fig 6C). However, K51A-mutant Myc-tagged RIPK3, which lacks kinase activity (He et al, 2009), does not induce MLKL recruitment (Fig 6C). To further confirm the role of RIPK3 in Mtb-induced necrosis, we examined cell viability (Fig 6D), cell death mechanisms (Figs 6E and EV4C), and Mtb growth rate (Fig 6F) in RIPK3-overexpressing $Socs6^{-/-}$ BMDMs. The results showed that recruitment of RIPK3 to RIPK1 contributed to the switch from apoptosis to necrosis in Mtb-stimulated BMDMs. We then knocked down RIPK3 or MLKL with siRNAs in Mtb-stimulated $Socs6^{+/+}$ BMDMs and found that RIPK3 and MLKL were both required for complex formation (Fig EV4D). Furthermore, Mtb-induced necrosis was attenuated upon knockdown of RIPK3 or MLKL in Mtb-stimulated $Socs6^{+/+}$ BMDMs (Fig EV4E–H). However, unlike RIPK3, overexpression of MLKL alone did not alter necrosis in $Socs6^{-/-}$ BMDMs (Fig EV4I–K). Taken together, these data demonstrate that recruitment of RIPK3 to RIPK1 switches apoptosis to necrosis in Mtb-stimulated BMDMs.

A20 controls the degradation of RIPK3 through K48-linked ubiquitination

Since RIPK3 overexpression caused $Socs6^{-/-}$ BMDMs to switch from apoptosis to necrosis, we further investigated the RIPK3 degradation pathway. The degradation of RIPK3 was blocked by the proteasome inhibitor MG132 but not by lysosome protease inhibitors, such as E64d and pepstatin A (E64d/PepA) (Fig 7A). This indicated that RIPK3 undergoes proteasome-dependent rather than lysosome-dependent degradation. Both the miR-342-3p mimic and $Socs6$ siRNA facilitated RIPK3 ubiquitination and subsequent degradation in Mtb-stimulated $Socs6^{+/+}$ BMDMs (Fig 7B). Additionally, SOCS6 overexpression suppressed the ubiquitination of RIPK3 in Mtb-infected $Socs6^{-/-}$ BMDMs (Fig 7C).

It has been reported that RIPK3 can be modified by several E3 ligases, such as cIAP1/2, A20 (also known as TNFAIP3), and CHIP (Tenev et al, 2011; Onizawa et al, 2015; Seo et al, 2016). In this study, we found that A20 expression was correlated with RIPK3 ubiquitination levels (Fig 7B and C). More specifically, the ubiquitination of endogenous RIPK3 was suppressed by $A20$ siRNA (Fig 7D), while the ubiquitination of Flag-tagged RIPK3 was induced by A20 in RAW264.7 cells (Fig 7E). A20 directly targets RIPK3 for degradation through the in vitro ubiquitination system (Fig 7F). These data suggest that A20 is a direct E3 ligase of RIPK3.

The ovarian tumor (OTU) domain of A20 functions as a deubiquitinating (DUB) enzyme that hydrolyzes ubiquitin chains

(Onizawa et al, 2015). In addition to its DUB activity, A20 displayed E3 ubiquitin ligase activity that is mediated by seven Cys2-Cys2 zinc-finger (ZF) domains (Polykratis et al, 2019). This gives A20 dual ubiquitin editing capabilities. It is known that the C103A substitution in the OTU domain of A20 blocks deubiquitinating activity, whereas C609A and C612A substitutions in the zinc finger-4 (ZnF4) domain disrupt E3 ligase activity (Ma & Malynn, 2012; Lork & Beyaert, 2017). As shown in Fig 7G, introduction of C609A/C612A, but not C103A, blocked the ubiquitination of RIPK3, indicating that ZnF4 was responsible for catalyzing ubiquitination. In addition, a K51A kinase mutant of RIPK3 was unable to be ubiquitinated (Fig 7G), supporting the view that the kinase activity of RIPK3 is required for the formation of necrotic complexes. We also conducted RIPK3 binding studies with various A20 mutants to determine whether the ZnF4 domain contributes to the recognition of RIPK3. The results indicated that the A20 ZnF4 region was essential for RIPK3 binding (Appendix Fig S2A and B). To precisely define the ubiquitination of RIPK3, we cotransfected RIPK3 with A20 and ubiquitin mutants, where only K48 and/or K63 were available for polymerization (Appendix Fig S2C). The results showed that both K48- and K63-linked ubiquitin chains contributed to A20-mediated RIPK3 ubiquitination (Appendix Fig S2D). Notably, unlike K48-linked ubiquitination, K63-linked ubiquitination is independent of RIPK3 proteasomal degradation (Appendix Fig S2E).

The A20-mediated cell death mechanism is independent of inflammatory responses

To understand the role of A20 in the miR-342/SOCS6-mediated immune response to Mtb infection, BMDMs from mice with different genotypes were infected with Mtb and measured the release of cytokines (TNF-α, IL-1, IL-6, CXCL15) and chemokines (Ccl5, Cxcl10, Icam1). The results showed that the release of cytokines and chemokines was significantly higher in $Socs6^{-/-}$ BMDMs than in $Socs6^{+/+}$ BMDMs (Fig 8A and B). There was no difference in the release of cytokines and chemokines in $Socs6^{-/-}$ BMDMs with and without A20 (Fig 8A and B). In addition, assays measuring cell death mechanisms (Fig 8C, Appendix Fig S3) and cell viability (Fig 8D) showed that, in A20-overexpressing or A20-knockout cells, SOCS6 expression had no impact on the mechanism of cell death. Taken together, these data indicated that A20-regulated RIPK3 ubiquitination and the formation of a death complex were independent of SOCS6-mediated cytokine and chemokine production in response to Mtb stimulation. Mtb growth results confirmed that the A20-mediated cell death mechanism switch and the SOCS6-mediated inflammatory response played synergistic roles in controlling Mtb replication: Cells with high expression of A20 and low expression of SOCS6 had the strongest resistance to Mtb (Fig 8E).

Figure 8. A20-mediated cell death mechanism is independent of inflammatory responses.

A, B   Production of cytokines TNF-α, IL-1, IL-6, CXCL15 (A), or chemokines Ccl5, Cxcl10, Icam1 (B) in the $A20^{-/-}Socs6^{+/+}$, $A20^{+/+}Socs6^{+/+}$, $A20^{-/-}Socs6^{-/-}$, and $A20^{+/+}Socs6^{-/-}$ BMDMs after Mtb stimulation. Data are shown as the mean ± SEM of $n = 3$ biological replicates.

C–E   Cell death mechanisms (C), cell viabilities (D), or Mtb growth rates (E) of $A20^{-/-}Socs6^{+/+}$, $A20^{+/+}Socs6^{+/+}$, $A20^{-/-}Socs6^{-/-}$, and $A20^{+/+}Socs6^{-/-}$ BMDMs stimulated with Mtb. Z-VAD treatment concentration was 20 μM, and the treatment time was 24 h. Data are shown as the mean ± SEM of $n = 3$ biological replicates.

F   Schematic representation of miR-342 regulated anti-Mtb immunity.

Data information: ANOVA followed by Bonferroni post hoc test (A-E) was used for data analysis. *$P < 0.05$, **$P < 0.01$. Abbreviation: n.s., not significant.
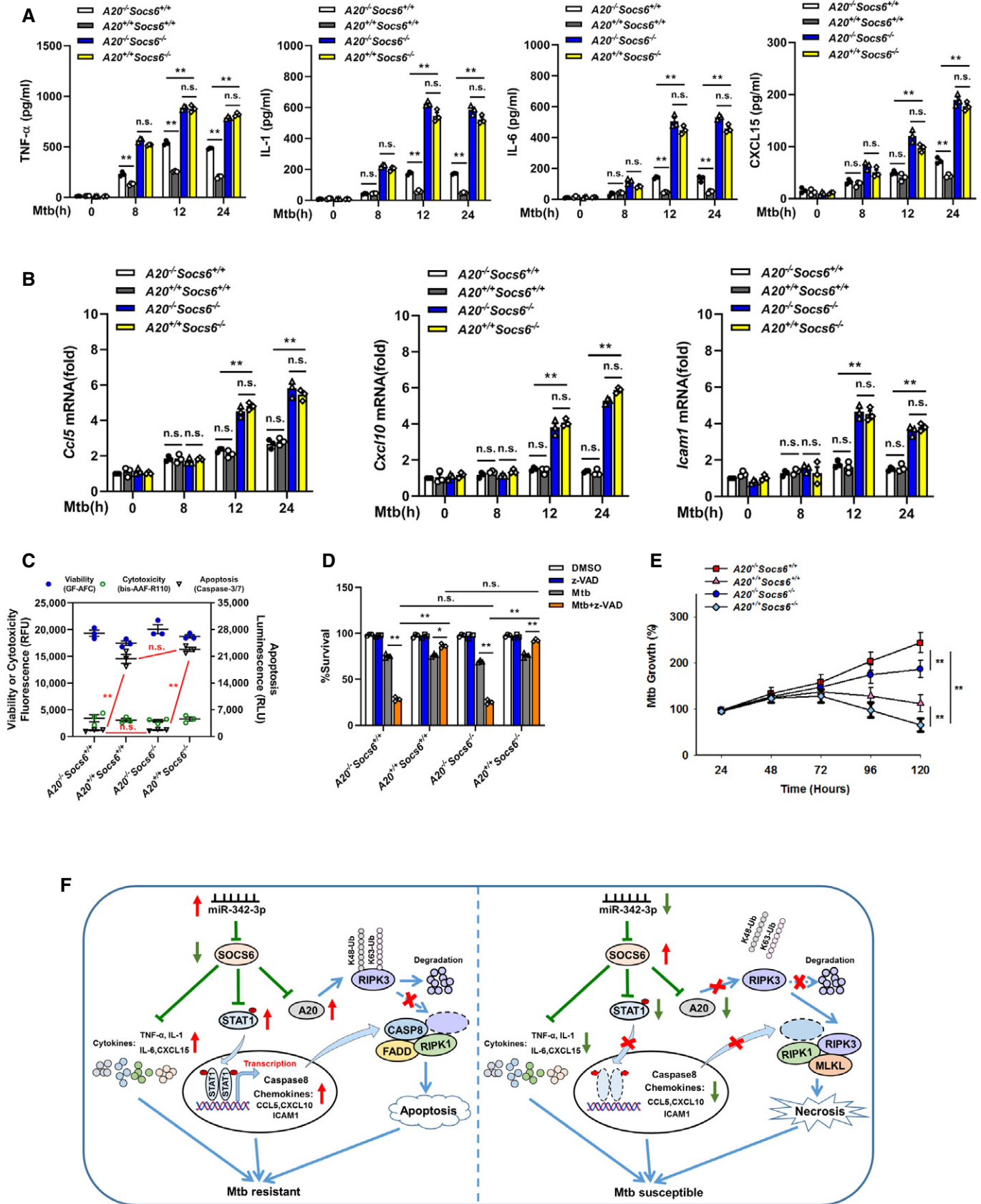
Figure 8.

In summary, our data show that the miR-342-3p/SOCS6 axis strengthens the anti-Mtb immune system by increasing the production of inflammatory cytokines and chemokines and by switching cell death from necrosis to apoptosis through A20-mediated K48 ubiquitination and RIPK3 degradation (Fig 8F).

Discussion

In this study, we found that SOCS6 is regulated by miR-342-3p and thus mediates multiple downstream immune response pathways. Considering that other SOCS family members have similar structures to SOCS6, we examined whether they could also be regulated by miR-342-3p. The results showed that miR-342-3p had no significant effect on the 3'UTR activity of other SOCS family members (Appendix Fig S4A), indicating that miR-342-3p has a relatively specific regulatory effect on SOCS6. We also examined the effects of SOCS6 on the regulation of other SOCS and STAT family members (Fig EV3A, Appendix Fig S4B–D). The results showed that SOCS6 negatively regulates the expression of SOCS7 (Appendix Fig S4B). However, siRNA knockdown experiments indicated that SOCS7 is dispensable for Mtb-induced cell death in C3H and B6 mice (Appendix Fig S4C and D). STAT3 activation was also observed in Mtb-infected $Socs6^{+/+}$ macrophages (Fig EV3A). A similar STAT3 activation pattern was also detected in $Socs6^{-/-}$ cells (Fig EV3A). Thus, we speculate that STAT3 activation has no effect on SOCS6 and that the pathway by which SOCS6 mediates downstream STAT1 is relatively independent of other STAT family members. However, this needs to be validated with further experiments.

Apoptosis and necrosis are two common forms of cell death that play essential roles in the development and maintenance of homeostasis in multicellular organisms (Green & Llambi, 2015). In Mtb-infected macrophages, necrosis is associated with uncontrollable cellular damage, providing a niche for Mtb replication before it escapes into the extracellular milieu (Lerner et al, 2017). Apoptosis, on the other hand, results in programmed cell suicide, thus limiting the replication of Mtb (Behar et al, 2011; Zhao et al, 2017). It has been reported that *in vitro* modulation of apoptosis affects mycobacterial cell-to-cell spread, suggesting an unambiguous relationship between apoptosis and the propagation of Mtb (Aguilo et al, 2013). We found that the recruitment of RIPK1 and FADD to caspase 8 resulted in apoptotic cell death in Mtb-infected macrophages. On the other hand, when the complex was formed with RIPK1, RIPK3, and MLKL, necrotic cell death was observed. This result is consistent with previous reports showing that RIPK3 acts as a molecular switch between TNF-induced apoptosis and necrosis in mouse embryonic fibroblasts and that high levels of RIPK3 can switch apoptosis into necrosis in certain cell types. Interestingly, Stutz et al (2018) argued that RIPK3 does not play a fundamental role in regulating inflammatory responses or necrosis *in vivo*. In our current work, we found that RIPK3 did not affect the production of several inflammatory cytokines, including TNF-α and IL-1, which is consistent with Stutz's findings. However, we also found that recruitment of RIPK3 to the cytoplasmic complex contributed to the necrosis of Mtb-infected macrophages. We hypothesize that SOCS6 may play as-yet undescribed roles in various aspects of macrophage activities, including activation, differentiation, and Mtb-induced cell death mechanisms.

Many bacterial pathogens exploit the host ubiquitination system to promote pathogenesis. For example, the host E3 ubiquitin ligase ANAPC2 interacts with mycobacterial protein Rv0222 to suppress the expression of pro-inflammatory cytokines (Wang et al, 2020). A20, an inhibitor of NF-κB signaling, has dual ubiquitination and deubiquitination roles within the proteasomal degradation pathway and is highly connected to the immune response network (Vereecke et al, 2009; Sokhi et al, 2018; Priem et al, 2020). A20 also contains seven ZF domains, which mediate its E3 ubiquitin ligase and ubiquitin-binding activities (Lork & Beyaert, 2017). We found that upregulation of A20 facilitates RIPK3 ubiquitination, resulting in apoptotic cell death in Mtb-stimulated macrophages. We also showed that the ZF4 domain is responsible for A20-mediated K48- and K63-linked ubiquitination of RIPK3. K48-linked ubiquitin chains tag substrates for proteasomal degradation, whereas K63-linked ubiquitin chains fulfill diverse proteasome-independent cellular roles, including endocytosis, DNA damage responses, and immune responses (Yau & Rape, 2016). Consistent with previous reports, we found that the proteasomal degradation of RIPK3 depended on K48 ubiquitination alone. However, the functional role of K63-linked ubiquitination of RIPK3 has not been fully elucidated. It would be interesting to further investigate the specific role of K63-ubiquitinated RIPK3 in determining the fate of macrophages.

Cytokines such as IL-1 mediate susceptibility to Mtb. $Mir342^{-/-}$ B6 mice, which were susceptible to Mtb, showed low levels of inflammatory factors (TNF-α, IL-1, IL-6, and CXCL15) along with severe lung lesions. Ji et al (2019) reported that IL-1 plays a protective role during Mtb infection, which is consistent with our results. Interestingly, they also found that elevated levels of IL-1α/β proteins in B6J.C3-$Sst1^{C3HeB/FeJKrmn}$ mice (which are susceptible to Mtb) failed to control Mtb (Ji et al, 2019). This difference might be due to the different genotypes of the mice used in these studies or the "double-edged sword" character of cytokines in the immune system.

The release of cytokines and chemokines was dramatically higher in $Socs6^{-/-}$ macrophages than in $Socs6^{+/+}$ macrophages. This suggested that A20 regulates the degradation of RIPK3 and that the induction of apoptosis is independent of SOCS6-mediated inflammatory responses. Interestingly, the presence or absence of A20 exerted different effects on cytokine release in $Socs6^{+/+}$ macrophages but not in $Socs6^{-/-}$ macrophages. We speculate that this may be because SOCS6 has a stronger inhibitory effect on cytokines than A20. Although A20 can be used as a negative feedback regulator of NF-κB to inhibit the production of cytokines, its effect is far smaller than that of SOCS6. Therefore, the absence of SOCS6 will result in a large increase in cytokine expression; in this case, the regulatory effect of A20 appears to be minimal. However, this hypothesis needs to be verified by further experiments.

C3H (TB susceptible) and B6 (TB resistant) inbred mice were used as models in this study. We found that the deletion of miR-342 in B6 mice resulted in susceptibility to Mtb infection, as evidenced by acceleration of bacterial load within organs and development of necrotic lung lesions. Additionally, we observed an inverse correlation between the expression of miR-342-3p and tuberculosis. These data indicate that miR-342-3p participates in a new regulatory pathway involved in tissue necrosis. Despite the substantial amount of work presented, there are still some limitations and remaining questions. For example, we performed miR-342-3p knockout in B6 mice

and miR-342-3p overexpression in C3H mice. Since the expression of miR-342-3p is not the only difference between these mouse strains, interventions (knockout and overexpression) performed in both strains would be better for direct comparisons. Next, we used macrophages derived from SOCS6-knockout C3H mice ($Socs6^{-/-}$) and their wild-type littermates ($Socs6^{+/+}$) as *in vitro* models to study the effects of SOCS6 on downstream signaling pathways and cell death mechanisms. Although the amount of SOCS6 protein was exquisitely manipulated by the interventions as expected (Appendix Fig S4E), these manipulations are not a perfect substitute for alterations in miR-342-3p levels. We also observed an inverse correlation between miR-342-3p expression and tuberculosis in clinical PBMC samples. Because other cell types may also serve as a source of miR-324-3p, we believe that using pure macrophages rather than PBMCs would provide a more convincing argument. In addition, PBMCs extracted from whole blood might not have even been in contact with Mtb. In the future, it would be worth investigating how the upregulation of miR-342-3p is initiated and whether it depends on direct contact with Mtb. We speculate that infection signals could be transmitted through cellular communication, such as endocrine communication, which means that the signals could be transmitted throughout the organism via the circulatory system. However, more clinical data and experiments are required to test this hypothesis. In this study, z-VAD, a pan-caspase inhibitor, was used to distinguish cell death mechanisms. A miR-342-3p inhibitor induced a switch from apoptosis to necrosis in Mtb-infected B6 BMDMs. Interestingly, cell survival was further decreased upon the addition of z-VAD. This observation is consistent with previous reports (He *et al*, 2009; Zhang *et al*, 2009). We speculate that, in addition to caspase inhibition, z-VAD might be involved in the regulation of cell death patterns via additional mechanisms. The potential roles of z-VAD in cell death require further investigation.

Materials and Methods

Ethic statements

This study was carried out in strict accordance with the Guidelines for the Care and Use of Animals of Chongqing University. All animal experimental procedures were approved by the Animal Ethics Committees of the School of Life Sciences, Chongqing University. Blood samples were obtained from Chongqing Public Health Medical Center in accordance with the guidelines of the local ethics committee. Patients providing blood samples were given informed consent. The ethics committee approved this consent procedure.

Mice

All animal study protocols were reviewed and approved by Chongqing University School of Life Sciences review boards for animal studies. C3HeB/FeJ and C57BL/6J mice were purchased from Jackson Laboratory. $Mir342^{+/+}$ C3H mice (C3HeB/FeJ-Tg (mROSA-Mir342)1cyagen) and $Mir342^{-/-}$ B6 mice (C57BL/6J-$Mir342^{\text{tm1cyagen}}$) were constructed and identified by Cyagen Biosciences (Guangzhou, China). Littermate wild-type mice were used as controls. Briefly, in order to generate $Mir342^{+/+}$ C3H mice, pre-miR-342 sequence was cloned into pBROAD3 vector and

transgenic mice were obtained by pronuclear microinjection. $Mir342^{-/-}$ B6 mice were generated as previously described (Dooley *et al*, 2017). The $Socs6^{-/-}$ mice (C3HeB/FeJ-$Socs6^{\text{em1cyagen}}$) were purchased from Cyagen Biosciences (Guangzhou, China). Littermate wild-type mice were used as controls. The pBROAD3-A20 vector was microinjected into the zygotes from $Socs6^{+/+}$ (wild-type) and $Socs6^{-/-}$ mice to generate A20-overexpressing mice ($A20^{+/+}Socs6^{+/+}$, $A20^{+/+}Socs6^{-/-}$). A20-knockout mice ($A20^{-/-}Socs6^{+/+}$, $A20^{-/-}Socs6^{-/-}$) were generated from $Socs6^{+/+}$ and $Socs6^{-/-}$ mice using CRISPR/Cas9.

Blood samples

TB patients ($n = 34$) were diagnosed based on clinical presentation and radiological signs and were confirmed by sputum culture positivity. Subjects were excluded if they had autoimmune disorders or other infectious diseases. The average age was 45, and 55.9% of patients were male. The control individuals ($n = 27$) came from healthy donors. The inclusion criteria were no previous history of TB, and no evidence of TB-related infiltration in chest X-rays. The average age was 42, and 51.9% of the controls were male. All protocols were approved by the local ethics committee of the Public Health Medical Center, Chongqing, China, and signed informed consent was obtained from subjects.

Plasmids construction

The 3′-UTR of *Socs6* (Genebank Accession number: NM_018821.5) was amplified and inserted the psicheck-2 vector (Promega) through standard molecular cloning methods and confirmed by sequencing. Full-length coding sequence of *Socs6* was inserted into pCDH-MCS-T2A-Puro-MSCV (System Biosciences, Palo Alto, CA, USA); the recombinant construct was named pCDH-SOCS6. The lentiviral vector pCDH-SOCS6 and packaging plasmids such as pMD2.G and psPAX2 were cotransfected into HEK-293T cells to generate lentivirus. The RIPK3 (Genebank Accession number: NM_019955.2) and A20 (Genebank Accession number: NM_009397.3) mutants were generated by overlapped extension PCR method based on wild-type plasmids. The K48R, K63R, and K48/63R mutants were kindly provided by Dr. Yonghui Zheng (Michigan State University). The wild-type Ubiquitin and other mutants were purchased from Addgene. All the primers used for plasmids construction are listed in Appendix Table S2.

Bacterial strains and infection

The Mycobacterial strain H37Rv (ATCC, Manassas, VA, USA) was grown in Middlebrook 7H9 (BD Biosciences, San Jose, CA, USA) medium supplemented with 10% OADC (BD Biosciences) and 0.05% Tween-80 (Sigma-Aldrich, St. Louis, MO, USA), or on Middlebrook 7H10 agar (BD Biosciences) supplemented with 10% OADC. For mice infection, 6-week-old mice were randomly allocated into groups and aerosol infected with approximately 400 CFU Mtb. The mice were killed at the indicated time. The organs were collected for CFU assay or histopathology analysis. All mice were age- and sex-matched in each experiment. Every effort was made to minimize animal pain, suffering, and distress and reduce the number of animals used.

In vivo transfection

The *in vivo* transfection of mice was performed by tail vein injection (N/P ratio = 8) using the jetPEI *in vivo* transfection reagent (Polyplus Transfection Inc, New York, NY, USA) according to the manufacturer's instruction as previously described (Sutherland *et al*, 2014; Li *et al*, 2016). Injections were repeated 3 times per week for the living mice.

Cell culture, transfection, and treatment

NIH-3T3, HEK-293T, and RAW264.7 cells were obtained from American Type Culture Collection (ATCC) and grown adherently to plastic plates (Corning Costar, Cambridge, MA, USA). The culture medium was composed of Dulbecco's modified Eagle's medium (DMEM, Gibco, USA) and 10% fetal bovine serum (Gibco). Double-stranded mmu-miR-342-3p (miRBase accession number MIMAT0000590, UCUCACACAGAAAUCGCACCCGU) mimic, single-stranded mmu-miR-342-3p inhibitor and their corresponding negative controls (NC mimic or inhibitor) were purchased from GenePharma (GenePharma, Shanghai, China). BMDMs were obtained by culturing bone marrow cells as previously described (Sutavani *et al*, 2018). In brief, bone marrow cells were cultured in RPMI-1640 (Gibco) supplemented with 10% heat-inactivated FBS, 2 mM L-glutamine, 1% nonessential amino acids, 100 unit penicillin, 100 μg streptomycin, and 22 ng M-CSF (PeproTech, Rocky Hill, NJ, USA)/ml for 6 d at 37°C, 5% CO_2. After 6 d of culture, adherent macrophages were switched into antibiotic-free media and seeded with 10^5 cells per well. BMDMs were infected with Mtb at a MOI of 5 for *in vitro* research. Human PBMCs were obtained by density gradient centrifugation (Ficoll, Sigma-Aldrich) from fresh heparinized whole blood. All cells were maintained in a humidified, 37°C incubator with 5% CO_2.

Identification of cell death mechanism

ApoTox-Glo Triplex Assay (Promega, Madison, WI, USA) was used to identify the cell death mechanism following manufactory instructions. In brief, GF-AFC and bis-AAF-R110 substrates were added to the cell culture medium. Cells were incubated for 30 min at 37°C, and fluorescence data were collected to assess viability and cytotoxicity. Then, 100 μl of Caspase-Glo 3/7 reagent was added to the mixture. Cells were incubated for 30 min at room temperature. Luminescence data were collected to assess the caspase activation. Apoptosis or necrosis result was determined according to the manual: Cell apoptotic death was with a high level of caspase activation, and cell necrotic death was with a low level of caspase activation. In addition, Annexin V/PI staining was also used to identify apoptotic and necrotic cells as previously described (Pan *et al*, 2005). Briefly, at indicated time points, cells were stained with Annexin V/PI (Sigma-Aldrich), fixed with 1% paraformaldehyde, and then analyzed using a BD LSR II flow cytometer (BD Biosciences). Data were analyzed with FlowJo data analysis software.

In vitro CFU assay

CFU assay was performed by plating tenfold serial dilutions of each tissue homogenate on Middlebrook 7H10 agar plates. The colonies were counted after 4–6 weeks of incubation at 37°C in 5% CO_2.

Histopathology analysis

Pathology scoring system was used in histopathology analysis as previously described with partial modification (Wu *et al*, 2015). Pathological changes of lung lobes were examined and evaluated by semiquantitative gross pathology scoring system: 0 = no visible lesions; 1 = no external gross lesions, but lesions seen upon slicing; 2 = less than five gross lesions with a diameter < 4 mm; 3 = more than five gross lesions with a diameter < 4 mm; 4 = more than one distinct gross lesion with a diameter > 4 mm; 5 = gross coalescing lesions. The scores of the individual lobes were added to calculate the lung score. Typical lesions were fixed with 10% buffered formaldehyde for more than 24 h, embedded in paraffin, sectioned, and stained with H&E according to the standard procedure. Photographs were obtained by microscopy (Carl Zeiss, Jena, Germany).

Immunoprecipitation and immunoblot analysis

Immunoblot analysis was performed as previously described (Fu *et al*, 2020b). Cell lysates were fractionated by sodium dodecyl sulfate polyacrylamide gel electrophoresis and transferred to polyvinylidene fluoride membranes (Millipore, Bedford, MA, USA). Blots were probed with 1/1,000 anti-SOCS6 (PA5-50263), 1/1,000 anti-STAT1 (AHO0832), 1/500 anti-phospho-STAT1 (44-376G) (Thermo Fisher Scientific, San Jose, CA, USA), 1/500 anti-Ubiquitin (sc-271289), 1/500 anti-HA (sc-7392), 1/500 anti-Myc (sc-56634), 1/500 anti-Caspase 8 (sc-5263, 1/30 for IP), 1/500 anti-CXCL10 (sc-374092), 1/500 anti-ICAM1 (sc-18853), 1/500 anti-CCL5 (sc-373984), 1/500 anti-STAT3 (sc-8019), 1/500 anti-phospho-STAT3 (sc-8059), 1/500 anti-STAT4 (sc-398228), 1/500 anti-phospho-STAT4 (sc-28296), 1/500 anti-STAT6 (sc-374021), 1/500 anti-phospho-STAT6 (sc-136019), 1/500 anti-SOCS1 (sc-518028), 1/500 anti-SOCS3 (sc-73045), 1/500 anti-SOCS4 (sc-135566), 1/500 anti-SOCS5 (sc-100858), 1/500 anti-SOCS7 (sc-137241), 1/200 anti-Caspase 2 (sc-53928), 1/200 anti-Caspase 9 (sc-56076) (Santa Cruz Biotechnology, Santa Cruz, CA, USA), 1/1,000 anti-MLKL (SAB1302339), 1/1,000 anti-RIPK1 (SAB3500420) (Sigma-Aldrich), 1/1,000 anti-RIPK3 (NBP1-77299, 1/200 for IP) (Novus Biologicals, Englewood, CO, USA), 1/500 anti-STAT2 (72604), 1/500 anti-phospho-STAT2 (88410), 1/500 anti-STAT5 (25653), 1/500 anti-phospho-STAT5 (9359), 1/500 anti-SOCS2 (2779) (Cell Signaling Technology, Inc., Danvers, MA, USA), 1/1,000 anti-Actin (AA128), and 1/1,000 anti-Flag (AF519, 1/100 for IP) (Beyotime, Jiangsu, China) antibodies. Immunoblots were revealed using SuperSignal west pico substrate (Thermo Fisher Scientific). The relative intensity of protein bands was quantified using ImageJ software and normalized to controls. For IP, cells were collected and lysed with 1× lysis buffer (Thermo Fisher Scientific), and afterward, the lysates were incubated with appropriate antibodies and Protein A/G beads (Thermo Fisher Scientific) at 4°C overnight. The beads were washed three times with IP buffer (Thermo Fisher Scientific), followed by immunoblot analysis.

Luciferase assays

Luciferase assays were performed using the Dual-Luciferase Reporter (DLR) Assay System (Promega) as previously described (Wu *et al*, 2015). In brief, cells were cotransfected with luciferase

reporter plasmid and internal control plasmid pRL-SV40. Cells were lysed for DLR assays 24 h after treatment. Data were collected with a VICTOR X5 Multilabel Plate Reader (PerkinElmer, Waltham, MA, USA) and relative luciferase activities were measured by firefly luciferase luminescence divided by renilla luciferase luminescence.

Cell viability assays

Cell viability was performed using a Cell Titer-Glo Luminescent Cell Viability Assay kit (Promega) following manufactory instructions. In brief, 100 μl of Cell Titer-glo reagent was added to the cell culture medium. Cells were then incubated at room temperature for 10 min. Luminescent data were collected with a VICTOR X5 Multilabel Plate Reader (PerkinElmer).

Real-time qRT–PCR

We used qRT–PCR to analyze gene expression. Total RNA samples were isolated using TRIzol reagent (Invitrogen, Life Technologies, CA, USA). Purified RNA was reverse-transcribed using a SYBR PrimeScript RT–PCR Kit (Takara, Otsu, Shiga, Japan). The expression of mRNAs was quantified using a SYBR Premix ExTaq II Kit (Takara). qRT–PCR was performed on Bio-Rad CFX-96 system (Bio-Rad, Hercules, CA, USA), and results were normalized to *β-actin* mRNA levels. We also used qRT–PCR to analyze miRNA expression. Total RNA samples were isolated using mirVana miRNA Isolation Kit (Ambion, Austin, TX, USA). Purified RNA was reverse-transcribed using a miScript II RT Kit (Qiagen, Hilden, Germany). The expressions of mature miRNAs were quantified using a miScript SYBR Green PCR Kit, which contained 10× miScript Universal Primer (Qiagen), and were performed according to the manufacturer's instructions. Quantization of U6 was performed to normalize miRNA expression levels. Data were analyzed using the $2^{-\Delta\Delta Ct}$ method. All primer sequences used for qRT–PCR are listed in Appendix Table S3.

Enzyme-linked immunosorbent assays

RAW264.7 and BMDMs were infected with Mtb for the indicated periods of time, and equal volumes of control and infected culture supernatants cleared by centrifugation were assayed by ELISA. TNF-α, IL-1, IL-6, and CXCL15 ELISA kits were purchased from e-Biosciences (Thermo Fisher Scientific). The concentration of each cytokine was calculated against a standard curve.

Statistical analysis

Sample size was based on empirical data from pilot experiments. The investigators were blinded during data collection and analysis. Data are presented as mean ± SEM and analyzed by ANOVA with Bonferroni post *hoc* test unless otherwise indicated. A value of $P < 0.05$ was considered significant.

Data availability

No primary data sets were generated and deposited.

Expanded View for this article is available online.

Author contributions

HW, XW, and ZL conceived and designed the study. HW, BF, XL, ST, RZ, WX, HZ, Shanfu. Z, QZ, YW, KF, LS, Shaolin. Z, WN, and KCP performed the experiments. HW, XW, and ZL analyzed the data. HW and BF wrote the manuscript. All authors read and approved the final manuscript.

Conflict of interest

The authors declare that they have no conflict of interest.

References

Aguilo JI, Alonso H, Uranga S, Marinova D, Arbues A, de Martino A, Anel A, Monzon M, Badiola J, Pardo J *et al* (2013) ESX-1-induced apoptosis is involved in cell-to-cell spread of *Mycobacterium tuberculosis*. *Cell Microbiol* 15: 1994–2005

Alexander WS, Hilton DJ (2004) The role of suppressors of cytokine signaling (SOCS) proteins in regulation of the immune response. *Annu Rev Immunol* 22: 503–529

Bartel DP (2018) Metazoan microRNAs. *Cell* 173: 20–51

Behar SM, Martin CJ, Booty MG, Nishimura T, Zhao X, Gan H, Divangahi M, Remold HG (2011) Apoptosis is an innate defense function of macrophages against *Mycobacterium tuberculosis*. *Mucosal Immunol* 4: 279–287

Carow B, Gao Y, Teran G, Yang XO, Dong C, Yoshimura A, Rottenberg ME (2017) CISH controls bacterial burden early after infection with *Mycobacterium tuberculosis* in mice. *Tuberculosis* 107: 175–180

Chakaya J, Khan M, Ntoumi F, Aklillu E, Razia F, Mwaba P, Kapata N, Mfinanga S, Hasnain SE, Katoto PD *et al* (2021) Global Tuberculosis Report 2020 - Reflections on the Global TB burden, treatment and prevention efforts. *Int J Infect Dis* https://doi.org/10.1016/j.ijid.2021.02.107

Choy EY, Siu KL, Kok KH, Lung RW, Tsang CM, To KF, Kwong DL, Tsao SW, Jin DY (2008) An Epstein-Barr virus-encoded microRNA targets PUMA to promote host cell survival. *J Exp Med* 205: 2551–2560

Dooley J, Lagou V, Pasciuto E, Linterman MA, Prosser HM, Himmelreich U, Liston A (2017) No functional role for microRNA-342 in a mouse model of pancreatic acinar carcinoma. *Front Oncol* 7: 101

Fu B, Xue W, Zhang H, Zhang R, Feldman K, Zhao Q, Zhang S, Shi L, Pavani KC, Nian W *et al* (2020a) MicroRNA-325-3p facilitates immune escape of *Mycobacterium tuberculosis* through targeting LNX1 via NEK6 accumulation to promote anti-apoptotic STAT3 signaling. *MBio* 11: e00557–e1520

Fu B, Yin S, Lin X, Shi L, Wang Y, Zhang S, Zhao Q, Li Z, Yang Y, Wu H (2020b) PTPN14 aggravates inflammation through promoting proteasomal degradation of SOCS7 in acute liver failure. *Cell Death Dis* 11: 803

Fulda S, Debatin KM (2002) IFNgamma sensitizes for apoptosis by upregulating caspase-8 expression through the Stat1 pathway. *Oncogene* 21: 2295 – 2308

Green DR, Llambi F (2015) Cell Death Signaling. *Cold Spring Harb Perspect Biol* 7: a006080

He SD, Wang L, Miao L, Wang T, Du FH, Zhao LP, Wang XD (2009) Receptor interacting protein kinase-3 determines cellular necrotic response to TNF-alpha. *Cell* 137: 1100 – 1111

Hong JY, Chung K-S, Shin J-S, Lee J-H, Gil H-S, Lee H-H, Choi E, Choi J-H, Hassan AHE, Lee YS *et al* (2019) The Anti-proliferative activity of the hybrid TMS-TMF-4f compound against human cervical cancer involves apoptosis mediated by STAT3 inactivation. *Cancers* 11: 1927

Huang J, Wang F, Argyris E, Chen K, Liang Z, Tian H, Huang W, Squires K, Verlinghieri G, Zhang H (2007) Cellular microRNAs contribute to HIV-1 latency in resting primary CD4+ T lymphocytes. *Nat Med* 13: 1241 – 1247

Iwakawa HO, Tomari Y (2015) The functions of microRNAs: mRNA decay and translational repression. *Trends Cell Biol* 25: 651 – 665

Ji DX, Yamashiro LH, Chen KJ, Mukaida N, Kramnik I, Darwin KH, Vance RE (2019) Type I interferon-driven susceptibility to *Mycobacterium tuberculosis* is mediated by IL-1Ra. *Nat Microbiol* 4: 2128 – 2135

Jonas S, Izaurralde E (2015) Towards a molecular understanding of microRNA-mediated gene silencing. *Nat Rev Genet* 16: 421 – 433

Jopling CL, Yi M, Lancaster AM, Lemon SM, Sarnow P (2005) Modulation of hepatitis C virus RNA abundance by a liver-specific microRNA. *Science* 309: 1577 – 1581

Kim D, Nguyen QT, Lee J, Lee SH, Janocha A, Kim S, Le HT, Dvorina N, Weiss K, Cameron MJ *et al* (2020) Anti-inflammatory roles of glucocorticoids are mediated by Foxp3(+) regulatory T cells via a miR-342-dependent mechanism. *Immunity* 53: 581 – 596.e5

Kim M, Shin DI, Choi BH, Min BH (2021) Exosomes from IL-1beta-primed mesenchymal stem cells inhibited IL-1beta- and TNF-alpha-mediated inflammatory responses in osteoarthritic SW982 cells. *Tissue Eng Regen Med* https://doi.org/10.1007/s13770-020-00324-x

Kramnik I (2008) Genetic dissection of host resistance to *Mycobacterium tuberculosis*: the sst1 locus and the Ipr1 gene. *Curr Top Microbiol Immunol* 321: 123 – 148

Kramnik I, Dietrich WF, Demant P, Bloom BR (2000) Genetic control of resistance to experimental infection with virulent *Mycobacterium tuberculosis*. *Proc Natl Acad Sci USA* 97: 8560 – 8565

Kumar M, Sahu SK, Kumar R, Subuddhi A, Maji RK, Jana K, Gupta P, Raffetseder J, Lerm M, Ghosh Z *et al* (2015) MicroRNA let-7 modulates the immune response to *Mycobacterium tuberculosis* infection via control of A20, an inhibitor of the NF-kappaB pathway. *Cell Host Microbe* 17: 345 – 356

Lerner TR, Borel S, Greenwood DJ, Repnik U, Russell MR, Herbst S, Jones ML, Collinson LM, Griffiths G, Gutierrez MG (2017) *Mycobacterium tuberculosis* replicates within necrotic human macrophages. *J Cell Biol* 216: 583 – 594

Leu JS, Chen ML, Chang SY, Yu SL, Lin CW, Wang H, Chen WC, Chang CH, Wang JY, Lee LN *et al* (2017) SP110b controls host immunity and susceptibility to tuberculosis. *Am J Respir Crit Care Med* 195: 369 – 382

Li X, He S, Li R, Zhou X, Zhang S, Yu M, Ye Y, Wang Y, Huang C, Wu M (2016) *Pseudomonas aeruginosa* infection augments inflammation through miR-301b repression of c-Myb-mediated immune activation and infiltration. *Nat Microbiol* 1: 16132

Liu F, Chen J, Wang P, Li H, Zhou Y, Liu H, Liu Z, Zheng R, Wang L, Yang H *et al* (2018) MicroRNA-27a controls the intracellular survival of *Mycobacterium tuberculosis* by regulating calcium-associated autophagy. *Nat Commun* 9: 4295

Liu S, da Cunha AP, Rezende RM, Cialic R, Wei Z, Bry L, Comstock LE, Gandhi R, Weiner HL (2016) The host shapes the gut microbiota via fecal microRNA. *Cell Host Microbe* 19: 32 – 43

Lork MVK, Beyaert R (2017) CYLD, A20 and OTULIN deubiquitinases in NF-kappa B signaling and cell death: so similar, yet so different. *Cell Death Differ* 24: 1172 – 1183

Ma A, Malynn BA (2012) A20: linking a complex regulator of ubiquitylation to immunity and human disease. *Nat Rev Immunol* 12: 774 – 785

Manca C, Tsenova L, Freeman S, Barczak AK, Tovey M, Murray PJ, Barry C, Kaplan G (2005) Hypervirulent *M. tuberculosis* W/Beijing strains upregulate type I IFNs and increase expression of negative regulators of the Jak-Stat pathway. *J Interferon Cytokine Res* 25: 694 – 701

Masood KI, Hussain R, Rao N, Rottenberg ME, Salahuddin N, Irfan M, Hasan Z (2014) Differential early secreted antigen target (ESAT) 6 kDa-induced IFN-gamma and SOCS1 expression distinguishes latent and active tuberculosis. *J Infect Dev Ctries* 8: 59 – 66

Masood KI, Rottenberg ME, Carow B, Rao N, Ashraf M, Hussain R, Hasan Z (2012) SOCS1 gene expression is increased in severe pulmonary tuberculosis. *Scand J Immunol* 76: 398 – 404

Masood KI, Rottenberg ME, Salahuddin N, Irfan M, Rao N, Carow B, Islam M, Hussain R, Hasan Z (2013) Expression of *M. tuberculosis*-induced suppressor of cytokine signaling (SOCS) 1, SOCS3, FoxP3 and secretion of IL-6 associates with differing clinical severity of tuberculosis. *BMC Infect Dis* 13: 13

Onizawa M, Oshima S, Schulze-Topphoff U, Oses-Prieto JA, Lu T, Tavares R, Prodhomme T, Duong B, Whang MI, Advincula R *et al* (2015) The ubiquitin-modifying enzyme A20 restricts ubiquitination of the kinase RIPK3 and protects cells from necroptosis. *Nat Immunol* 16: 618 – 627

O'Shea JJ, Schwartz DM, Villarino AV, Gadina M, McInnes IB, Laurence A (2015) The JAK-STAT pathway: impact on human disease and therapeutic intervention. *Annu Rev Med* 66: 311 – 328

Pan H, Yan BS, Rojas M, Shebzukhov YV, Zhou H, Kobzik L, Higgins DE, Daly MJ, Bloom BR, Kramnik I (2005) Ipr1 gene mediates innate immunity to tuberculosis. *Nature* 434: 767 – 772

Polykratis A, Martens A, Eren RO, Shirasaki Y, Yamagishi M, Yamaguchi Y, Uemura S, Miura M, Holzmann B, Kollias G *et al* (2019) A20 prevents inflammasome-dependent arthritis by inhibiting macrophage necroptosis through its ZnF7 ubiquitin-binding domain. *Nat Cell Biol* : 731 – 742

Priem D, van Loo G, Bertrand MJM (2020) A20 and cell death-driven inflammation. *Trends Immunol* 41: 421 – 435

Qu C, Xu QS, Lu MM, Wang FF, Liu ZQ, Liu DY, Yang W, Yi QL, Wang LL, Song LS (2018) The involvement of suppressor of cytokine signaling 6 (SOCS6) in immune response of Chinese mitten crab *Eriocheir sinensis*. *Fish Shellfish Immunol* 72: 502 – 509

Seo J, Lee E-W, Sung H, Seong D, Dondelinger Y, Shin J, Jeong M, Lee H-K, Kim J-H, Han SY *et al* (2016) CHIP controls necroptosis through ubiquitylation- and lysosome-dependent degradation of RIPK3. *Nat Cell Biol* 18: 291 – 302

Sironi JJ, Ouchi T (2004) STAT1-induced apoptosis is mediated by caspases 2, 3, and 7. *J Biol Chem* 279: 4066 – 4074

Sokhi UK, Liber MP, Frye L, Park S, Kang K, Pannellini T, Zhao B, Norinsky R, Ivashkiv LB, Gong S (2018) Dissection and function of autoimmunity-associated TNFAIP3 (A20) gene enhancers in humanized mouse models. *Nat Commun* 9: 658

Song M, Ping Y, Zhang K, Yang L, Li F, Zhang C, Cheng S, Yue D, Maimela NR, Qu J *et al* (2019) Low-dose IFNgamma induces tumor cell stemness in tumor microenvironment of non-small cell lung cancer. *Cancer Res* 79: 3737 – 3748

Stutz MD, Ojaimi S, Ebert G, Pellegrini M (2018) Is receptor-Interacting protein kinase 3 a viable therapeutic target for *Mycobacterium tuberculosis* infection? *Front Immunol* 9: 1178

Sullivan CS, Grundhoff AT, Tevethia S, Pipas JM, Ganem D (2005) SV40-encoded microRNAs regulate viral gene expression and reduce susceptibility to cytotoxic T cells. *Nature* 435: 682−686

Sutavani RV, Phair IR, Barker R, McFarlane A, Shpiro N, Lang S, Woodland A, Arthur JSC (2018) Differential control of Toll-like receptor 4-induced interleukin-10 induction in macrophages and B cells reveals a role for p90 ribosomal S6 kinases. *J Biol Chem* 293: 2302−2317

Sutherland TE, Logan N, Ruckerl D, Humbles AA, Allan SM, Papayannopoulos V, Stockinger B, Maizels RM, Allen JE (2014) Chitinase-like proteins promote IL-17-mediated neutrophilia in a tradeoff between nematode killing and host damage. *Nat Immunol* 15: 1116−1125

Tenev T, Bianchi K, Darding M, Broemer M, Langlais C, Wallberg F, Zachariou A, Lopez J, MacFarlane M, Cain K *et al* (2011) The ripoptosome, a signaling platform that assembles in response to genotoxic stress and loss of IAPs. *Mol Cell* 43: 432−448

Vereecke L, Beyaert R, van Loo G (2009) The ubiquitin-editing enzyme A20 (TNFAIP3) is a central regulator of immunopathology. *Trends Immunol* 30: 383−391

Wang L, Wu J, Li J, Yang H, Tang T, Liang H, Zuo M, Wang J, Liu H, Liu F *et al* (2020) Host-mediated ubiquitination of a mycobacterial protein suppresses immunity. *Nature* 577: 682−688

Wang L, Xia JW, Ke ZP, Zhang BH (2019) Blockade of NEAT1 represses inflammation response and lipid uptake via modulating miR-342-3p in human macrophages THP-1 cells. *J Cell Physiol* 234: 5319−5326

Wu H, Wang Y, Zhang Y, Yang M, Lv J, Liu J, Zhang Y (2015) TALE nickase-mediated SP110 knockin endows cattle with increased resistance to tuberculosis. *Proc Natl Acad Sci USA* 112: E1530−1539

Wu Y, Guo Z, Yao K, Miao Y, Liang S, Liu F, Wang Y, Zhang Y (2016) The transcriptional foundations of Sp110-mediated macrophage (RAW264.7) Resistance to *Mycobacterium tuberculosis* H37Ra. *Sci Rep* 6: 22041

Yau R, Rape M (2016) The increasing complexity of the ubiquitin code. *Nat Cell Biol* 18: 579−586

Yoshimura A, Naka T, Kubo M (2007) SOCS proteins, cytokine signalling and immune regulation. *Nat Rev Immunol* 7: 454−465

Zhang DW, Shao J, Lin J, Zhang N, Lu BJ, Lin SC, Dong MQ, Han JH (2009) RIP3, an energy metabolism regulator that switches TNF-induced cell death from apoptosis to necrosis. *Science* 325: 332−336

Zhao X, Khan N, Gan H, Tzelepis F, Nishimura T, Park SY, Divangahi M, Remold HG (2017) Bcl-xL mediates RIPK3-dependent necrosis in *M. tuberculosis*-infected macrophages. *Mucosal Immunol* 10: 1553−1568